ADVANCING EARTH AND SPACE SCIENCES

Global Biogeochemical Cycles®

RESEARCH ARTICLE
10.1029/2024GB008261

Key Points:

- The total GHG emissions in South Asia increased by 34%–43% during the 2010s compared to the 2000s
- The region's GHG emissions in the 2010s from the TD (4,532 ± 807.5 Tg CO_2 eq) and BU models (4,517 ± 639.8 Tg CO_2 eq) were compared well
- In the 2010s, terrestrial ecosystems acted as CO_2 sinks, though the sink was much smaller than the total carbon emissions

Supporting Information:

Supporting Information may be found in the online version of this article.

Correspondence to:

A. K. Jain,
jain1@illinois.edu

Citation:

Jain, A. K., Seshadri, S., Anand, J., Chandra, N., Patra, P. K., Canadell, J. G., et al. (2025). South Asia's ecosystems are a net carbon sink, but the region is a major net GHG source to the atmosphere. *Global Biogeochemical Cycles*, *39*, e2024GB008261. https://doi.org/10.1029/2024GB008261

Received 6 JUN 2024
Accepted 31 MAR 2025

Author Contributions:

Conceptualization: Atul K. Jain
Data curation: Seetharaman Seshadri, Naveen Chandra, Prabir K. Patra, Naiqing Pan
Formal analysis: Atul K. Jain
Funding acquisition: Atul K. Jain
Investigation: Atul K. Jain
Methodology: Atul K. Jain, Jatin Anand
Project administration: Atul K. Jain
Supervision: Atul K. Jain
Visualization: Abha Chhabra, Murali K. Gumma, Him Lal Shrestha, Baktiar N. Siddiqui
Writing – original draft: Atul K. Jain
Writing – review & editing: Atul K. Jain, Seetharaman Seshadri, Jatin Anand, Prabir

South Asia's Ecosystems Are a Net Carbon Sink, But the Region Is a Major Net GHG Source to the Atmosphere

Atul K. Jain[1], Seetharaman Seshadri[1], Jatin Anand[1], Naveen Chandra[2], Prabir K. Patra[2,3], Josep G. Canadell[4], Abha Chhabra[5], Philippe Ciais[6], Hammad Gilani[7], Murali K. Gumma[8], Masayuki Kondo[9], Erandathie Lokupitiya[10], Naiqing Pan[11], Him Lal Shrestha[12], Baktiar N. Siddiqui[13], Hanqin Tian[11], and Yogesh K. Tiwari[14]

[1]Department of Climate, Meteorology, and Atmospheric Sciences (CLiMAS), University of Illinois Urbana-Champaign, Urbana, IL, USA, [2]Research Institute for Global Change, JAMSTEC, Yokohama, Japan, [3]Research Institute for Humanity and Nature, Kyoto, Japan, [4]Global Carbon Project, Commonwealth Scientific and Industrial Research Organisation, Environment, Canberra, ACT, Australia, [5]Indian Space Research Organisation (ISRO), Ahmedabad, India, [6]Laboratoire des Sciences du Climat et de l'Environnement, CEA CNRS UVSQ UPSaclay, Gif-sur-Yvette, France, [7]International Water Management Institute, Lahore, Pakistan, [8]Geospatial Sciences and Big Data, International Crops Research Institute for the Semi-Arid Tropics (ICRISAT), Patancheru, Telangana, India, [9]The IDEC Institute - Center for Peaceful and Sustainable Futures (CEPEAS), Network for Education and Research on Peace and Sustainability (NERPS), Seto Inland Sea Carbon Neutral Research Center (S-CNC), Graduate School of Humanities and Social Sciences International Economic Development Program (IEDP), Graduate School of Innovation and Practice for Smart Society (SmaSo), Hiroshima University, Higashi-Hiroshima, Japan, [10]University of Colombo, Colombo, Sri Lanka, [11]Department of Earth and Environmental Sciences, Center for Earth System Science and Global Sustainability, Schiller Institute for Integrated Science and Society, Boston College, Chestnut Hill, MA, USA, [12]Kathmandu Forestry College, Kathmandu, Nepal, [13]Arannayk Foundation, Dhaka, Bangladesh, [14]Indian Institute of Tropical Meteorology, Ministry of Earth Sciences Govt of India, Pune, India

Abstract As part of the REgional Carbon Cycle Assessment and Processes-2 (RECCAP-2) project of the Global Carbon Project, here we estimate the GHG budgets (anthropogenic and natural sources and sinks) for the South Asia (SA) region as a whole and each country (Afghanistan, Bangladesh, Bhutan, India, Nepal, Pakistan, and Sri Lanka) for the decade of 2010–2019 (2010s). Countries in the region are experiencing a rapid rise in fossil fuel consumption and demand for agricultural land, leading to increased deforestation and higher greenhouse gas emissions. This study synthesizes top-down (TD) and bottom-up (BU) dynamic global vegetation model results, BU GHG inventories, ground-based observation upscaling, and direct emissions for major GHGs. The fluxes for carbon dioxide (CO_2), methane (CH_4), and nitrous oxide (N_2O) analyzed include fossil fuel emissions, net biome productivity, land use change, inland waters, wetlands, and upland and submerged soils. Our analysis shows that the overall total GHG emissions contributed to a net increase of 34%–43% during the 2010s compared to the 2000s, primarily driven by industrial activities. However, terrestrial ecosystems acted as a notable exception by serving as a CO_2 sink in the 2010s, effectively sequestering atmospheric carbon. The sink was significantly smaller than overall carbon emissions. Overall, the 2010s GHG emissions based on BU and TD were 4,517 ± 639.8 and 4,532 ± 807.5 Tg CO_2 eq, with CO_2, CH_4, and N_2O emissions of 2165.2 ± 297.1, 1,404 ± 95.9, and 712 ± 466 Tg CO_2 eq based on BU models 2,125 ± 515.1, 1,531 ± 205.2, and 876 ± 446.0 Tg CO_2 eq based on TD models. Total emissions from SA in the 2010s accounted for approximately 8% of the global share. The terrestrial CO_2 sinks estimated by the BU and TD models were 462.9 ± 195.5 and 210.0 ± 630.4 Tg CO_2, respectively. Among the SA countries, India was the largest emitter contributing to 80% of the region's total GHG emissions, followed by Pakistan (10%) and Bangladesh (7%).

Plain Language Summary South Asia (SA) is among the largest tropical and sub-tropical areas and has extensive industrial activity, producing a large quantity of greenhouse gases (GHGs). The region also has a lot of natural areas like forests, which both emit and absorb GHGs, making it hard to estimate how much GHGs are being released into the atmosphere overall. Thus, understanding how human activities and nature in SA contribute to more GHG emissions in the atmosphere and climate change is necessary for a deeper understanding of emission trends, their drivers, and GHG-climate feedback. Our study quantifies how much GHGs South Asian countries released into the atmosphere in the 2010s. Such country-specific information is crucial, especially for the Paris Climate Agreement (UNFCCC, 2015; https://unfccc.int/sites/default/files/english_paris_agreement.pdf), which asks countries to report exactly how much they're adding or taking away from the atmosphere. Our study focused on three main GHGs: CO2, CH4, and N2O. The study results showed

K. Patra, Josep G. Canadell, Philippe Ciais, Hammad Gilani, Masayuki Kondo, Erandathie Lokupitiya, Hanqin Tian, Yogesh K. Tiwari

that the GHG budget was the net source of the atmosphere during the 2010s. However, terrestrial ecosystems acted as a notable exception by serving as a net CO2 sink, effectively sequestering atmospheric carbon.

1. Introduction

South Asia (SA) has experienced rapid environmental transformations over the last few decades due to population growth, the green revolution, industrialization, and deforestation. With ballooning populations and fast-growing economies, these countries will likely undergo further development and increase energy production using fossil fuels. It is noted that the rapid Gross Domestic Product (GDP) growth in SA increased energy demand and its dependence on fossil fuels as a source of energy. SA contributed 9.3% of global emissions in 2019, with India alone responsible for 7.3% (Crippa, Guizzardi et al., 2020; Crippa, Solazzo et al., 2020).

Geographically, SA is one of the biggest tropical areas covering an area of 5.13×10^6 km^2. The region has a high variability of terrestrial sources and sinks (Cervarich et al., 2016), which makes estimating temporal trends in net terrestrial GHG emissions challenging. Thus, a more profound knowledge of how SA ecosystems respond to different environmental factors, such as climate change and atmospheric CO_2, is necessary for a deeper understanding of trends, their drivers, and carbon-climate feedback.

SA has also experienced increasing food demand, resulting in significant land use land cover changes (LULCCs), such as intensive agriculture, overgrazing, and converting forest land to agricultural land (Xu et al., 2021). There are much concern about how these rapid alterations in LULCC activities affect the volume of litter deposition, soil organic matter, and vegetation. Thus, these alterations have important yet uncertain implications for regional carbon and other GHG budgets.

Furthermore, forest fires significantly affect the GHG budget by rapidly releasing carbon and other GHGs stored within vegetation. Studies have shown that SA emissions from fires, resulting from both land-use and non-land-use changes, are approximately 422 ± 230 Tg CO_2 per year, accounting for about 6% of global fire emissions averaged over the period 1997–2016 (van der Werf et al., 2017). The emissions due to only non-land-use changes were 60 ± 33 Tg CO_2/yr (van der Werf et al., 2017), showing notable interannual variability. These fires, which both human activities and natural phenomena can trigger, often result in simultaneous emissions from biomass sources.

The region significantly contributes to CH_4 emissions, primarily due to rice cultivation (Gumma et al., 2011) and livestock (Xu et al., 2021). Following the Green Revolution (Pingali, 2012), CH_4 emissions have surged, driven by the widespread adoption of high-yielding crop varieties, intensified usage of nitrogen fertilizers, and the expansion of agricultural lands to meet the escalating food demands of SA's growing population. Long-term atmospheric data show that industrial and agricultural activities have significantly enhanced the emissions of CH_4 to the atmosphere (e.g., Dlugokencky et al., 2011; Etheridge et al., 1992; Ghosh et al., 2015).

SA has also become one of the world's epicenters within the hotspots of nitrous oxides (N_2O) and nitrogen (N) pollution (Raghuram et al., 2021; Tian et al., 2020, 2024). Growing food and energy demands of an increasing population have increased anthropogenic N_2O emissions from farming, waste production, and burning of fossil fuels in the world's energy, transportation, industrial, urban, and other sectors.

Climate change is modifying the emissions and fluxes of these GHGs and the underlying environmental conditions of the region. According to previous studies (Cervarich et al., 2016; Friedlingstein et al., 2022; IPCC, 2021; Patra et al., 2013), SA currently contributes 8%–10% of the annual global GHG emissions of the Planet and faces greater challenges in meeting nationally determined contributions (NDC) made at COP26 (UNFCCC, 2021) in a scenario of rapid economic growth and increasing demands for goods and services. However, for mitigation to be effective, an accurate estimation of not only CO_2 emissions but also non-CO_2 GHG emissions is needed.

This study expands and builds upon previous research (Cervarich et al., 2016; Friedlingstein et al., 2022; Patra et al., 2013) by delving deeper into the budget analysis of the three major GHGs (CO_2, CH_4, and N_2O) for the SA and provides a comprehensive assessment of their distribution across each country of the region.

10.1029/2024GB008261

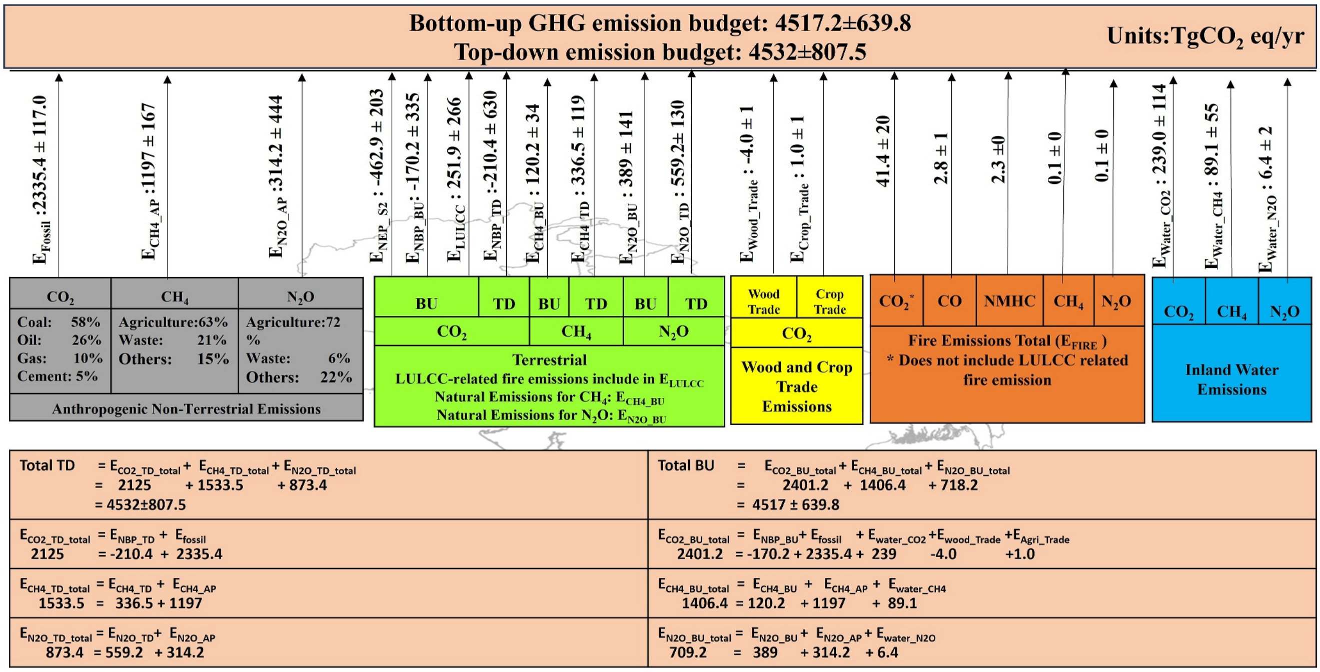

Figure 1. Emissions from anthropogenic, terrestrial (anthropogenic for CO_2, CH_4, and N_2O and natural for N_2O and CH_4), wood and crop trade, fire, and inland water for the South Asian region. The bottom panel shows the equations for calculating CO_2, CH_4, and N_2O based on the Top-Down (TD) and Bottom-Up (BU) models described in Section 2.7.

This study quantifies country-specific net GHG fluxes to help assess their net GHG contributions to the atmosphere. Such country-level estimates are crucial, especially within the 2015 Paris Climate Agreement (UNFCCC, 2015), which requires explicit quantification of GHG sources and sinks at the national level to effectively enact climate policies.

We report the GHG budget, which includes CO_2, CH_4, and N_2O, and its spatial as well as decadal variability for SA and each contributing country (Afghanistan, Bangladesh, Bhutan, India, Nepal, Pakistan, and Sri Lanka) for the period 2010–2019 (hereafter 2010s), a RECCAP-2 standard study period, and compare the 2010s with the previous decade (2000s) results. We report results for countries in the region that occupy 12 or more $0.5° \times 0.5°$ grid cells. The Maldives is the only country that does not meet this criterion. The number of $0.5° \times 0.5°$grid cells and % area share of SA covering each of the remaining seven countries are as follows: Afghanistan (244, 12%), Bangladesh (40, 2%), Bhutan (12, 1%), India (1,144, 63%), Nepal (52, 3%), Pakistan (328, 17%), and Sri Lanka (24, 1%). The study is part of an effort to study South Asia's GHG balance under the umbrella of the 2nd phase of the REgional Carbon Cycle Assessment and Processes (RECCAP-2), an initiative within the framework of the international Global Carbon Project (www.globalcarbonproject.org/reccap/, Ciais et al., 2022).

2. Materials and Methods

We synthesize GHG fluxes from terrestrial and non-terrestrial pools. The terrestrial fluxes account for anthropogenic emissions, particularly LULCC emissions (E_{LULC}), and natural GHG sources and sinks. In contrast, the non-terrestrial fluxes account for fossil fuel and anthropogenic emissions involving all industrial activities for CO_2, CH_4, and N_2O (Figure 1). To do so, we combine the outputs of different models and data products, including (a) results of dynamic global vegetation models (DGVMs) as the bottom-up approach (hereafter BU), (b) atmospheric inversion model as the top-down approach (hereafter TD), fossil fuels, fire, riverin induced CO_2, CH_4 and N_2O fluxes exchanged with the atmosphere, and wood and crop trade fluxes, and remote sensing data products, (c) a book-keeping model results to assess carbon fluxes and terrestrial carbon budgets.

The BU models typically run at $0.5° \times 0.5°$, whereas the TD models run at relatively coarse resolutions. It is not straightforward to define the resolution of TD models, which involve (1) forward transport models (typically has a spatial resolution of $2.5° \times 2.5°$), and inverse models for flux optimization at the forward model grid level with an

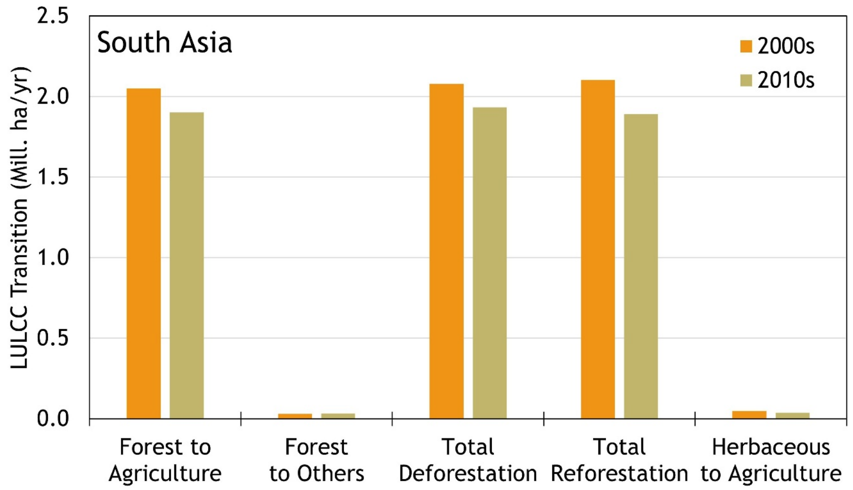

Figure 2. The land use and land cover change transitions for South Asia for the 2000s and 2010s.

assumption of 1,000 km or wider flux a priori spatial correlation or solves, for example, about 84 independent regions in matrix method. The temporal resolution for BU models varies from hourly to daily resolution. TD models range from weekly to monthly time intervals, depending on the model design and data availability. For this study, we compile results at 0.5° × 0.5° spatial resolution and yearly temporal resolution for 2000–2019. If data for a model output is not available for the entire decade of the 2010s, we calculate the mean of the available years and use it as a representative value for the 2010s.

2.1. CO_2 Fluxes From Terrestrial Ecosystems

2.1.1. Estimates of Net Biome Production (NBP) Based on the Bottom-Up Approach

The Net Biome Production (NBP) based on the bottom-up (BU) approach (E_{NBP_BU}) was calculated using the following equation:

$$E_{NBP\_BU} = E_{NEP\_S2} - E_{LULCC} - E_{Fire}$$

where E_{NEP_S2} is net terrestrial ecosystem production flux, LULCC emissions, E_{LULCC} emissions, and E_{Fire} fire emissions due to non-LULCC activities, the methods for calculating each of these terms are described next.

We used an ensemble of 16 DGVM (BU) results based on TRENDY Version 11 (Friedlingstein et al., 2022; details of each model are in Table S1 in Supporting Information S1) for two different simulation scenarios, S2 and S3, for the calculations of E_{NEP_S2} and E_{LULCC} (Figure 1). Model simulations followed the protocol described by the Global Carbon Project (TRENDY) (Sitch et al., 2015), where each model was run from its pre-industrial equilibrium (beginning of 1700) to 2021. For S2 simulations, which calculate E_{NEP_S2} (= GPP [gross primary productivity]—Ra [autotrophic respirations] —Rh [heterotrophic respiration]), the models were forced with changing CO_2 (Dlugokencky & Tans, 2022), CRU-JRA reanalysis climate forcing (Viovy, 2018), and time-invariant pre-industrial (the year 1700) land use data (LUH2; Goldewijk et al., 2017) over the period 1700–2021. In the S3 simulations, which calculated E_{S3} (=E_{NEP_S2} + E_{LULCC}), the same input for CO_2 and climate as for the S2 case was assumed, but the LULCC varied with time based on HYDE3.2 and LUH2 data sets over the period 1700–2021. E_{LULCC} was estimated by subtracting E_{NEP_S2} from E_{S3}. All DGVMs accounted for major LULCC activities, such as clearing the forest for croplands and other ecosystems and forest regrowth (Figure 2), as well as the decomposition of dead organic matter associated with natural cycles and the vegetation and soil carbon response to increasing atmospheric CO_2 concentration and climate change. Some models explicitly simulate the coupling of carbon and nitrogen cycles and account for atmospheric N deposition and N fertilizer data of Tian et al. (2020) (Table S1 in Supporting Information S1).

The E_{LULCC} term accounted for fire emissions due to LULCC activities, such as deforestation fires. The fire emission term (E_{Fire}) accounted for CO_2 emissions due to non-LULCC related fire activities, such as wildfires as well as fire emissions for carbon monoxide (CO), CH_4, and non-methane hydrocarbons (NMHCs) for all fire-related activities, including LULCC, based on an updated version of GFED v4.1 data (van der Werf et al., 2017). This data was based on global fire emissions from various sources such as deforestation, savanna, forest, agricultural, and peat fires. GFED v4.1 combines long-term time series of satellite-derived data for the burned area, fire activity, and plant productivity with CASA (Carnegie–Ames–Stanford approach) model-estimated results for fuel loads and combustion completeness (van der Werf et al., 2017). The data was available for 1997–2019 on their website (http://globalfiredata.org). Here, we used the data for 2000–2019 to calculate $E_{Fire}$for 2000s and 2010s.

2.1.2. Estimates of NBP Based on Top-Down Approach

Top-down estimates of NBP (E_{NBP_TD}) (i.e., inclusive of all non-fossil CO2 fluxes exchanged between the land and the atmosphere) were estimated using the ensemble of seven inversion model results based on TRENDY Version 11 (Friedlingstein et al., 2022); details of inversion models are provided in Table S2 in Supporting Information S1). All inversion models employ the Bayesian synthesis method and use atmospheric CO_2 data to the end of 2019 to infer the spatiotemporal distribution of the CO_2 flux exchanged between the atmosphere and the land along with prior fluxes for fossil fuels, land biospheres, fires, and oceanic exchange (Friedlingstein et al., 2022; Patra et al., 2013). The variations between different model results are mainly due to the choice of atmospheric CO_2 and historical flux data, the spatial resolution, the estimated correlation structures, and the mathematical approach of the models (Deng et al., 2022; Friedlingstein et al., 2022).

2.2. CH_4 Emissions

The bottom-up terrestrial flux estimates for CH_4 emissions account for wetland fluxes calculated using the ensemble of six DGVMs model results (details of each in Table S3 of Supporting Information S1), inland water fluxes based on the synthesis of different model results (Section 2.4), and anthropogenic fluxes from the EDGAR_v7.0 (Crippa, Guizzardi et al., 2020; Crippa, Solazzo et al., 2020) (Section 2.5). The DGVMs calculations account for processes important for CH_4 fluxes, including CH_4 production, oxidation, and transport, as well as the data for long and shortwave radiation, air pressure, specific humidity, total precipitation, air temperature, and wind speed and direction (Melton et al., 2013; Poulter et al., 2017; Saunois et al., 2020). CH_4 fluxes are calculated as a product of the area, and the model estimates the emission flux density. The DGVMs were run for the period 2000–2017 using the dynamic wetland area data set prescribed from satellite data on inundated areas without lakes and inland waters (WAD2M, Saunois et al., 2020). The BU estimates do not account for CH_4 sink from upland and emissions from termites.

The top-down inversion model estimates are based on global inversions (Chandra et al., 2021), a model of atmospheric chemistry and transport, and a prior distribution of methane sinks and sources and their uncertainties to postulate improved methane sinks and sources estimates. Here, we employed an ensemble of eight atmospheric inversion model results for CH_4 emission fluxes (Saunois et al., 2020), which use global Eulerian transport models (details of each are given in Table S4 in Supporting Information S1). The models combine all the elements of the methane cycle, including atmospheric CH_4 observations, emissions and sinks on the earth's surface, and air temperature distribution in the atmosphere, to calculate temperature-dependent loss rates from reactions with OH radicals. In addition, prior emission flux information is derived from BU approaches, for example, process-based models or from the interpolation of available data (natural sources) and various inventories (anthropogenic sources) (Houweling et al., 2017; Saunois et al., 2020).

2.3. Soil N_2O Emission Fluxes

2.3.1. Bottom-Up Estimates

The bottom-up terrestrial N_2O soil emissions were estimated based on the ensemble of seven DGVMs model results (details of each in Table S5 in Supporting Information S1) for 2010–2019, which were obtained from the N_2O Model Intercomparison Project (NMIP) (Tian et al., 2020). To quantify the magnitude and pattern of N_2O fluxes, the ecosystem models require various input data sets, which include the atmospheric CO_2 concentration, climatic conditions (e.g., temperature and precipitations), LULCC, N deposition, synthetic N fertilizer input data for the crop and pastureland areas, and production and applications of manure N input for the crop and pastureland areas (Tian et al., 2020). All the model simulations started with the equilibrium carbon and N status in 1860. After that, models were transiently run from 1860 to 2020.

2.3.2. Top-Down Estimates for N_2O Emission Fluxes

In the present study, the ensemble of four N_2O atmospheric inversion model results based on Tian et al. (2020) was used to estimate N_2O fluxes (details of each are given in Table S6 in Supporting Information S1) for 2010–2016. Inversion models use N_2O measurements of discrete air samples from the National Oceanic and Atmospheric Administration (NOAA) Carbon Cycle Cooperative Global Air Sampling Network. A few sites of continuous measurements from the Japan Meteorological Agency (JMA) and the National Institute of Environmental Studies (NIES). Atmospheric N_2O measurements are the most sparse among the three species considered here because of the poor stability of the instrument for securing high precision (better than 0.2 ppb measurement uncertainty in 300 ppb) and long-term measurements.

2.4. CO_2, CH_4, and N_2O Emission Fluxes From Inland Waters

Emissions for CO_2 (E_{Water_CO2}), CH_4 (E_{Water_CH4}), and N_2O (E_{Water_N2O}) from inland water, including those from streams, rivers, lakes, and reservoirs, E_{Water_total} (Figure 1), were taken from Lauerwald et al. (2023a, 2023b), which calculate emissions for 10 RECCAP-2 regions, including SA. These emission estimates were based on the synthesis of existing estimates of GHG emissions from streams, rivers, lakes, and reservoirs but homogenized with regard to underlying global maps of water surface area distribution and the effects of seasonal ice cover. The study excluded emissions from smaller lentic water bodies, such as ponds as well as those from temporally inundated floodplains and swamps due to a lack of data on a global scale.

2.5. Fossil Fuels and Other Non-Terrestrial Anthropogenic Emissions for CO_2, CH_4, and N_2O

The anthropogenic non-terrestrial GHG emissions for SA countries were taken from the European Commission's Emissions Database for Global Atmospheric Research (EDGAR) data set (Crippa, Guizzardi et al., 2020; Crippa, Solazzo et al., 2020). We used EDGAR update data (EDGARv7.0) because it provides independent country- and sector-specific estimates of GHG emissions based on a robust and consistent methodology stemming from the latest IPCC guidelines and most recent activity data. The data was compiled from a number of international statistical sources (Crippa, Guizzardi et al., 2020; Crippa, Solazzo et al., 2020), providing estimates at the spatial scale for fossil fuel CO_2 emissions (E_{Fossil}, including burning of coal, oil, gas, and others (e.g., gas flaring), and cement production for each country for the period 1970–2021. Regarding CH_4 anthropogenic emissions (E_{CH4_AP}), all anthropogenic activities (Figure 1) leading to climate-relevant anthropogenic emissions are included, except for biomass/biofuel combustion in the power, industry, buildings, transport, and agricultural sectors, large-scale biomass burning, and LULCC. It is important to note that while CH_4 emissions from livestock are not explicitly calculated, they are included as part of the total agricultural emissions. Anthropogenic activities for N_2O emissions (E_{N2O_AP}) include industrial activities involving energy generation and consumption, construction and production, and direct and indirect emissions from manure management. The anthropogenic non-terrestrial CH_4 and N_2O emission data are available for 1970–2018.

2.6. Wood and Crop Product Trade

This study accounts for CO2 fluxes associated with international trade, that is, import minus export, of wood (E_{Wood_Trade}) and crop products (E_{Agri_Trade}) in SA. In the wood trade, we considered industrial round wood for emission calculation as international fuelwood trade, and charcoal was often used for domestic purposes and not for international trade. We used FAOSTAT (2024) for the import and export quantities of wood and crop products in cubic meters (m^3), which classified industrial wood into coniferous and non-coniferous woods and a total of 92 crop products. This data in m^3 was converted to Tg CO_2 using the methods described by Peters et al. (2012) for wood and Xu et al. (2021) for crop products. For industrial wood, the m^3 of wood was converted to dry-weight biomass using the factor 0.45 t m^{-3} for coniferous raw wood and 0.59 t m^{-3} for non-coniferous raw wood, and then to a ton of carbon using 0.45 t C t^{-1} biomass. For agriculture, the ton of biomass in m^3 was calculated for individual crops. The crop-specific factors that convert the volume of biomass to dry-weight biomass and carbon in tons were taken from (Xu et al., 2021).

2.7. Total GHG Emissions

Total CO_2, CH_4, and N_2O emissions based on the BU models were calculated by the following equations:

$$E_{CO2\_BU\_total} = E_{NBP\_BU} + E_{Fossil} + E_{Water\_CO2} + E_{Wood\_Trade} + E_{Agri\_Trade}$$

$$E_{CH4\_BU\_total} = E_{CH4\_BU} + E_{CH4\_AP} + E_{Water\_CH4}$$

$$E_{N2O\_BU\_total} = E_{N2O\_BU} + E_{N2O\_AP} + E_{Water\_N2O}$$

Total CO_2, CH_4, and N_2O emissions based on the TD models were calculated by the following equations:

$$E_{CO2\_TD\_total} = E_{NBP\_TD} + E_{Fossil}$$

$$E_{CH4\_TD\_total} = E_{CH4\_TD} + E_{CH4\_AP}$$

$$E_{N2O\_TD\_total} = E_{N2O\_TD} + E_{N2O\_AP}$$

Following the IPCC AR6 (Canadell et al., 2021), we used the 100-year global warming potentials (GWP) of CH_4-fossil (29.8), CH_4 -non-fossil (27), and N_2O (278) to combine all top-down and bottom-up GHG emissions to CO_2 equivalent (CO_2 eq). In the case of NMHCs, the emissions of NMHCs given in Tg NMHC yr^{-1} were converted to Tg C yr^{-1} using a ratio of 161/210 TgC/Tg NMHC (Hoor et al., 2009).

Next, we discuss the 2010s results. The positive values represent a land sink of carbon, and the negative values represent atmospheric emissions.

2.8. Uncertainty Analysis

While the ensemble mean often provides more accurate and reliable results than relying on individual models (IPCC, 2014; Meehl et al., 2007; Weigel et al., 2008), it's crucial to estimate the uncertainty between the different model results, which can help to understand the spread of the individual model results. The uncertainties in the TD and BU model estimated GHG budget were evaluated based on the error propagation method, accounting for the standard deviations (1σ) of the individual component of the budget fluxes resulting from the ensemble of multiple models. The goal was to quantify how uncertainties in the component fluxes, derived from multiple models, influence the overall uncertainty of the GHG budget estimate. The total uncertainty (σ) of the ensemble of the modeled budget was calculated as the square root of the sum of the squares of the uncertainties of the individual flux components (e.g., $\sigma_x; \sigma_y, etc.$), under the assumption that the errors in component fluxes are uncorrelated, that is, $\sigma = \sqrt{\sigma_x^2 + \sigma_y^2 + \ldots}$.

3. Results

3.1. Net Terrestrial Ecosystem Productivity (E_{NEP_S2})

The TRENDY model results based on the S2 scenario, which do not account for any LULCC disturbances over time, suggest that E_{NEP_S2} increased from −272 ± 166.4 $TgCO_2\ yr^{-1}$ in the 2000s to −462.9 ± 195.5 Tg $CO_2\ yr^{-1}$ in the 2010s (Figure 1) mainly because of the higher CO_2 fertilization effect. The results from individual models for E_{NEP_S2} also exhibit significant variation from a low of −199 Tg CO_2 eq yr^{-1} for the SDGVM model to a high of −989 Tg CO_2 eq yr^{-1} for the JSBACH model (Table S1 in Supporting Information S1). Regarding the individual country's NEP for the 2010s, the estimates reflected the size of the country. For example, India saw relatively higher estimates of −366.7 ± 188.9 $TgCO_2$ eq yr^{-1} or 80% of the total regional value, followed by Pakistan and Nepal with estimated values of −25.8 ± 14.6 Tg CO_2 eq yr^{-1} (5%) and −23.1 ± 10.8 $TgCO_2$ eq yr^{-1} (4%) (Table 1).

3.2. Emissions From Land-Use and Land Cover Change (E_{LULCC})

The estimated E_{LULCC} based on BU was the net carbon source of 251.9 ± 203.8 $TgCO_2\ yr^{-1}$ (Figure 1) for the 2010s (Figure 1 and Table 1). The emissions increased by 45% compared to the 2000s (173 ± 191.4 Tg $CO_2\ yr^{-1}$) due to reduced reforestation over the 2010s compared to the 2000s. The results consistently reflect each country's

Table 1
Country-Specific and South Asia (SA) Region Net Biome Production Fluxes Based on the Ensemble of the Top-Down (E_{NBP_TD}) and Bottom-Up (E_{NBP_BU}) TRENDY Model Results, Fossil Emission (E_{Fossil}), and Total Fluxes ($E_{CO2\_BU\_Total} = E_{NBP\_BU} + E_{Fossil}$ and $E_{CO2\_TD\_Total} = E_{NBP\_TD} + E_{Fossil}$) for the 2010s

Country/Region	E_{NEP_S2}	E_{LULCC}	E_{fire}	E_{NBP_BU}[a]	E_{NBP_TD}	E_{Fossil}	$E_{CO2\_BU\_Total}$	$E_{CO2\_TD\_Total}$
Afghanistan	−17.6 ± 10.2	1.9 ± 10.9	0.03 ± 0.01	−15.7 ± 14.9	−6.7 ± 22.4	13.1 ± 0.6	−2.6 ± 14.9	6.4 ± 22.4
Bangladesh	−14.8 ± 11.6	10.4 ± 13.8	0.1 ± 0.01	−4.3 ± 18	−4.0 ± 38.3	83.4 ± 4.2	79.4 ± 18.5	79.4 ± 38.5
Bhutan	−5.3 ± 4.1	3.2 ± 3.8	0.2 ± 0.02	−1.0 ± 3.8	−0.5 ± 7.4	1.01 ± 0.1	0.01 ± 3.8	0.5 ± 7.5
India	−366.7 ± 188.9	200.6 ± 201.7	34.5 ± 3.4	−131.6 ± 276.3	−163.8 ± 504.2	2038.4 ± 101.9	1906.8 ± 294.5	1874.6 ± 514.4
Nepal	−23.1 ± 10.8	11.0 ± 9.7	4.1 ± 0.4	−8 ± 14.5	−17.1 ± 71.3	12.8 ± 0.6	4.8 ± 14.5	−4.3 ± 71.3
Pakistan	−25.72 ± 14.6	11.4 ± 19.8	1.7 ± 0.1	−12.6 ± 24.5	−16.6 ± 43.7	177.3 ± 8.9	164.7 ± 26.0	160.7 ± 44.5
Sri Lanka	−9.7 ± 6.4	12.8 ± 6.4	0.8 ± 0.1	3.9 ± 9.0	−1.9 ± 12.5	9.4 ± 0.5	13.3 ± 9.0	8.5 ± 12.5
SA Total	−462.9 ± 190.5	251.9 ± 203.8	41.4 ± 3.4	−170.2 ± 279.0	−210.4 ± 504.9	2335.4 ± 102.4	2165.2 ± 297.1	2125.8 ± 515.1

Note. Positive values are the carbon source, and negative values are the carbon sink ($TgCO_2$/yr). [a]$E_{NBP\_BU} = E_{NEP\_S2} + E_{LULCC} + E_{Fire}$, where E_{NEP_S2} is net ecosystem productivity with LULCC, E_{LULCC}, CO_2 flux due to LULCC, and E_{fire} due to non-LULCC emissions flux.

LULCC transitions. The region's net emissions are mainly determined by land change activities in the three largest countries in the region, India, Pakistan, and Bangladesh, with India's emissions being the highest (200.6 ± 201.7 Tg CO_2 yr^{-1}, 85%) because it occupies around 70% of the total area, followed by Sri Lanka (12.8 ± 6.4 Tg CO_2 yr^{-1}, 5%) and Pakistan (11.4 ± 19.8 Tg CO_2 yr^{-1}, 4%) (Table 1). The rest of the countries combined contributed about 7% of the total LULCC emissions for the SA region.

The BU estimated results are also well within the range of the ensemble of three book-keeping model results E_{LULCC_BK}, BLUE (354 Tg CO_2 yr^{-1}; Hansis et al., 2015), OSCAR (77 Tg CO_2 yr^{-1}; Gasser et al., 2020) and H&N (−1.6 Tg CO_2 yr^{-1}; Houghton & Nassikas, 2017) (Table S7 in Supporting Information S1). However, the results show significant variations between low and high ranges of values for book-keeping (ranging from −2 to 77 Tg CO_2 yr^{-1}) and bottom-up (ranging from −14 to 518 Tg CO_2 yr^{-1}) model results. The exact causes of such significant differences are not clear. This may be due to the different LULCC inputs and modeling approaches used to estimate emissions.

3.3. Fire Emissions (E_{FIRE})

As per the GFED4.1, the SA region is not a significant source of CO_2 emission due to non-LULCC-related biomass burning (Figure 1). Out of about 7,674 ± 195 Tg CO_2 yr^{-1} of total global emissions due to open fires (i.e., a fire in which material is burned in an outdoor area) (van der Werf et al., 2017), only 46.7 ± 23.3 Tg CO_2 yr^{-1} (0.6% of the global total) are emitted from non-LULCC sources in the SA countries (Table 2), which was about a 19% increase compared to the 2000s. The total regional non-LULCC fire CO_2 emissions for the 2010s can be attributed to open forest fires (22.2 ± 11.4 Tg CO_2 yr^{-1}) and savanna burning (14.8 ± 2.7 Tg CO_2 yr^{-1}) for the 2010s. Peat land fire emissions were almost negligible in SA. Amongst the countries that contributed most to the regional non-LULCC emissions, India stands out with an estimated contribution of about 83% (39 ± 19.01 Tg CO_2 yr^{-1}), followed by Nepal 10% (4.5 ± 2.3 Tg CO_2 yr^{-1}) and Sri Lanka 1.9% (0.9 ± 0.4 Tg CO_2 yr^{-1}). Moreover, the rest of the countries in SA contributed about 5% (2.3 ± 1.1 Tg CO_2 yr^{-1}) to the total non-LULCC CO_2 emissions due to fire in the SA region in the 2010s (Table 2).

The contribution of carbon monoxide (CO) emissions due to open fire to the global emissions is quite low, only 2.81 ± 0.25 Tg CO_2 yr^{-1} (0.8% of the global total of CO emissions). Compared to the 2000s (2.38 ± 0.23 Tg CO_2 yr^{-1}), the CO emissions increased by 16%.

Much like the CO emission, the contribution of SA CH_4 (0.14 ± 0.07 Tg CO_2 eq yr^{-1}), NMHC (2.33 ± 0.23 Tg CO_2 eq yr^{-1}), and N_2O (0.01 ± 0.01 Tg CO_2 eq yr^{-1}) (Figure 1) emissions to the global fire emissions is relatively smaller (less than 1% of total emission) (Table 2).

3.4. Riverine Carbon Flux (E_{Water})

The synthesis of total inland water (streams, rivers, lakes, and reservoirs) GHG emissions was 334.3 ± 126.9 Tg CO_2 eq yr^{-1} (Figure 1), with a dominant contribution from CO_2 (E_{Water_CO2}) (72%) and CH_4 (26%) (E_{Water_CH4})

Table 2
Country-Specific Fire Activity Related Emissions ($TgCO_2$ eq/yr) for CO_2, CO, NMHCs, CH_4, and N_2O for the 2010s

Country	CO_2[a]	CO	NMHCs	CH_4	N_2O	Total
Afghanistan	0.03 ± 0.01	0.00 ± 0.0	0.00 ± 0.0	0.00 ± 0.0	0.00 ± 0.0	0.03 ± 0.01
Bangladesh	0.10 ± 0.5	0.00 ± 0.0	0.01 ± 0.01	0.00 ± 0.0	0.00 ± 0.0	0.11 ± 0.05
Bhutan	0.22 ± 0.1	0.01 ± 0.01	0.01 ± 0.01	0.00 ± 0.0	0.00 ± 0.0	0.24 ± 0.1
India	34.54 ± 17.0	2.37 ± 0.23	1.98 ± 0.1	0.12 ± 0.01	0.01 ± 0.0	39.01 ± 19.5
Nepal	4.07 ± 2	0.24 ± 0.02	0.18 ± 0.02	0.01 ± 0.0	0.00 ± 0.0	4.51 ± 2.7
Pakistan	1.71 ± 0.9	0.11 ± 0.05	0.10 ± 0.01	0.01 ± 0.0	0.00 ± 0.0	1.93 ± 0.9
Sri Lanka	0.76 ± 0.4	0.06 ± 0.03	0.05 ± 0.01	0.00 ± 0.0	0.00 ± 0.0	0.88 ± 0.4
SA Total	41.43 ± 3.4	2.81 ± 0.3	2.33 ± 0.2	0.14 ± 0.01	0.01 ± 0.01	46.71 ± 23.4

[a]Fire emissions due to non-land use change-related fire activities.

and a minor contribution from N_2O (2%) (E_{Water_N2O}). The rivers were the most significant contributor to the regional inland water emissions (~85%), with minor contributions from reservoirs (10%) and lakes (5%). The most significant contributors to SA inland water GHG emissions were India (296.5 ± 112.6), Pakistan (23.4 ± 8.9), and Bangladesh (9 ± 3.6). These three countries account for more than 98% of the inland water GHG emissions (Table 3).

3.5. NBP (E_{NBP})

The BU models estimated E_{NBP_BU} (−170.2 ± 279.0 Tg CO_2 yr^{-1}), and the TD models estimated E_{NBP_TD} (−210.4 ± 504.9) Tg CO_2 yr^{-1} (Figure 1) show that the region acted as a net sink during the 2010s. Compared to the 2000s (BU: −99.0 ± 170.08 Tg CO_2 yr^{-1}; TD: −157.8 ± 581 Tg CO_2 yr^{-1}), the sink in the BU case increased by 72%, whereas in the case of TP, the increase was only about 33%. The ensemble of different TD and BU models suggests large uncertainties in the estimated CO_2 fluxes. With regard to the individual country's terrestrial carbon fluxes in 2010s, the terrestrial ecosystems acted as a sink for atmospheric CO_2, with India having the greatest sink, being the largest country of SA, for both modeling approaches (E_{NBP_BU}: 131.6 ± 276.3 Tg CO_2 yr^{-1} and E_{NBP_TD}: 163 ± 504 Tg CO_2 yr^{-1}) with relatively higher estimates of E_{NEP_S2} of 366.7 ± 188.9 Tg CO_2 yr^{-1} (Table 1).

3.6. CH_4 and N_2O Emissions From Soils

The estimates for the soil CH_4 emissions for the top-down models, E_{CH4_TD} (12.5 ± 4.4 Tg CH_4 yr^{-1}), are larger than the bottom-up emissions, E_{CH4_BU} (4.45 ± 1.27 Tg CH_4 yr^{-1}), with the emissions almost 2.8 times higher for the 2010s (Table 4). India had the maximum share in CH_4 emission in the SA for E_{CH4_TD} and E_{CH4_BU} cases, with an estimated contribution of 76% and 65% (Table 4). Compared to the 2000s, E_{CH4_TD} and E_{CH4_BU} emissions decreased by 12% and 8% in the 2010s.

The estimates for the soil N_2O emissions from the TD (E_{N2O_TD}) and BU (E_{N2O_BU}) models gave similar results for the SA region for the 2010s, with values of 2.0 ± 0.1 and 1.4 ± 0.5 Tg N yr^{-1} (Table 5). For both modeling approaches, India's emissions were the highest (78%–82%), followed by Pakistan (ca. 23%–25%) and Bangladesh (ca. 4%–6%). Compared to 2000s, the 2010s E_{N2O_TD} increased 73%, whereas E_{N2O_BU} 16%.

Table 3
Inland Water Emissions for CO_2, CH_4 and N_2O ($TgCO_2$ eq/yr)

Country	E_{Water_CO2}	E_{Water_CH4}	E_{Water_N2O}	Country total
Afghanistan	0.02 ± 0.0	0.01 ± 0.0	0.00 ± 0.0	0.03 ± 0.0
Bangladesh	6.09 ± 3.2	2.49 ± 1.6	0.18 ± 0.1	9.36 ± 3.6
Bhutan	0.31 ± 0.2	0.12 ± 0.1	0.01 ± 0.0	0.43 ± 0.2
India	211.92 ± 101.2	79.00 ± 49.4	5.60 ± 2.0	296.52 ± 112.6
Nepal	2.75 ± 1.3	1.02 ± 0.6	0.07 ± 0.0	3.85 ± 1.4
Pakistan	16.75 ± 8.0	6.25 ± 3.9	0.44 ± 0.2	23.40 ± 8.9
Sri Lanka	0.57 ± 0.3	0.21 ± 0.1	0.02 ± 0.0	0.80 ± 0.4
SA Total	239.0 ± 114.0	89.1 ± 55.7	6.3 ± 2.2	334.3 ± 126.9

3.7. Non-Terrestrial Anthropogenic Emissions for CO_2, CH_4, and N_2O

The estimated total non-terrestrial anthropogenic emissions for three GHGs in the 2010s were 3848 ± 506 Tg CO_2 eq yr^{-1} (Figure 1). CO_2 (E_{Fossil}), CH_4 (E_{CH4_AP}), and N_2O (E_{N2O_AP}) contributed 61%, 31%, and 8%, respectively. The following describes the emissions specific to each country and details the contributions of various anthropogenic activities.

Table 4
Estimated CH_4 Emissions (Tg CH_4/yr) From the Soils From Bottom-Up Models (E_{CH4_BU}) and Top-Down Models (E_{CH4_TD}) and From Anthropogenic Activities (E_{CH4_AP}) in South Asian Countries for the 2010s

Country	E_{CH4_AP}	E_{CH4_BU}	E_{CH4_TD}
Afghanistan	0.65 ± 0.10	0.01 ± 0.01	0.03 ± 0.1
Bangladesh	3.9 ± 0.60	0.72 ± 0.53	3.4 ± 1.6
Bhutan	0.02 ± 0.00	0.03 ± 0.00	0.07 ± 0.20
India	30.06 ± 4.50	3.38 ± 0.84	8.09 ± 3.11
Nepal	1.17 ± 0.30	0.03 ± 0.01	0.30 ± 0.22
Pakistan	7.98 ± 1.20	0.15 ± 0.03	0.37 ± 0.42
Sri Lanka	0.51 ± 0.10	0.10 ± 0.06	0.12 ± 0.10
SA Total	44.33 ± 6.20	4.45 ± 1.27	12.45 ± 4.4

3.7.1. CO_2 Emissions From Fossil Fuels and Cement Production (E_{Fossil})

Carbon emissions from burning fossil fuels, including cement production, have increased in the 2010s compared to the 2000s in every country of the SA region, according to the EDGAR data set (Crippa et al., 2021; Minx et al., 2021). The total regional emissions increased in the 2010s by 87%, from an average of 1,341 ± 67.5 Tg CO_2 yr^{-1} for the decade of the 2000s to an average of 2335.4 ± 102.4 Tg CO_2 yr^{-1} for the 2010s (Table 1) (Figure 1). The rapid increase in fossil CO_2 emissions was primarily attributed to the rapid economic growth. It is noted that the SA fossil fuel emissions grew at a higher rate than the GDP during the 2010s, wherein the GDP increased by $1,726 billion or by 16% in 2010s compared to the 2000s (World Bank, 2023) (Table S8 in Supporting Information S1). On the country scale, India's emissions were the highest (2,038 ± 101.9 CO_2 yr^{-1}) (87%), followed by Pakistan (177 ± 8.9 CO_2 yr^{-1}) (7%) and Bangladesh (83 ± 4.2 CO_2 yr^{-1}) (3%) during the 2010s (Table 6). Regarding percentage increase, Afghanistan, Bhutan, Bangladesh, and Nepal witnessed an increase of more than 100% in the 2010s relative to the 2000s. The contribution of individual countries to total fossil fuel emissions is also coherent with their contribution to the total regional GDP (Table S8 in Supporting Information S1).

The comparison between the EDGAR data set (Crippa et al., 2021; Minx et al., 2021) and the GCP (Friedlingstein et al., 2022) data set for fossil fuel emissions for the SA region exhibits excellent agreement across different countries; the emissions lie within the close range, with the average total emissions for EDGAR being only 3.4% higher than GCP (Table 6).

3.7.2. Non-Terrestrial Anthropogenic Emissions for CH_4 (E_{CH4_AP}) and N_2O (E_{N2O_AP})

The regional E_{CH4_AP} for the 2010s was 44.33 ± 6.20 Tg CH_4 yr^{-1}, about 76% and 90% of the total CH_4 emission estimates of TD and BU models. India generated the overwhelming majority of CH_4 in the regional budget, accounting for 68% (30.06 ± 4.50 Tg CH_4 yr^{-1}) of total anthropogenic CH_4 emissions. Pakistan and Bangladesh

Table 5
Estimated N_2O Emissions From Anthropogenic Activities (E_{N2O_AP}) and the Soils and From Bottom-Up Models (E_{N2O_BU}) and Top-Down Models (E_{N2O_TD}) in South Asian Countries for the 2010s (Tg N_2O/yr)

	E_{N2O_AP}	E_{N2O_BU}	E_{N2O_TD}
Afghanistan	0.02 ± 0.03	0.02 ± 0.02	0.06 ± 0.02
Bangladesh	0.06 ± 0.1	0.06 ± 0.03	0.08 ± 0.02
Bhutan	0.00 ± 0.0	0.00 ± 0.00	0.01 ± 0.00
India	0.84 ± 1.1	1.15 ± 0.4	1.64 ± 0.4
Nepal	0.02 ± 0.0	0.03 ± 0.01	0.06 ± 0.01
Pakistan	0.18 ± 0.2	0.13 ± 0.1	0.25 ± 0.10
Sri Lanka	0.01 ± 0.0	0.02 ± 0.00	0.01 ± 0.01
SA Total	1.13 ± 1.6	1.43 ± 0.51	2.1 ± 0.47

Table 6
Fossil Fuel CO_2 Emissions, E_{Fossil}, From EDGAR (Crippa et al., 2021) and Global Carbon Project (Friedlingstein et al., 2022) for the 2010s ($TgCO_2/yr$)

	E_{Fossil}	
Country	EDGAR	GCP
Afghanistan	13.1	9.2
Bangladesh	83.4	71.6
Bhutan	1.0	1.1
India	2038.4	2195.0
Nepal	12.8	8.0
Pakistan	177.3	187.1
Sri Lanka	9.4	19.0
Total	2335.4	2419.2

were the second and third largest contributors, with an estimated 18% (7.98 ± 1.20 $TgCH_4$ yr^{-1}) and 9% (3.9 ± 0.60 $TgCH_4$ yr^{-1}). Emissions from agriculture and waste played a predominant role in the anthropogenic sources of CH_4, with about 85% followed by fossil fuels, biomass, and biofuel burning.

The regional E_{N2O_AP} were 1.13 ± 1.6 Tg N_2O yr^{-1}, about 36% and 44% of total N_2O emissions estimated by TD and BU models. Again, India was the highest emitter (74%) of anthropogenic emissions, followed by Pakistan (16%). The rest of the countries' total emissions were only 10%. Anthropogenic emissions from direct sources, including fossils and industrial sources, biomass burning, and waste and wastewater, contributed the most to the total emissions (60%).

3.8. Wood (E_{Wood_Trade}) and Crop Trade (E_{Agri_Trade}) Emissions

The SA emissions from the international wood trade were -5 ± 1.0 Tg CO_2 yr^{-1}. India was the highest emitter -4.7 ± 0.9 $TgCO_2$ yr^{-1}. The regional emissions from the international crop trade were about 1.0 ± 0.2 Tg CO_2 yr^{-1}. The non-coniferous and coniferous roundwoood emissions were about -3.5 ± 0.6 Tg CO_2 yr^{-1} and -1.5 ± 0.3 Tg CO_2 yr^{-1}, respectively. Rice (0.3 ± 0.06 Tg CO_2 yr^{-1}), wheat products (0.17 ± 0.02 $TgCO_2$ yr^{-1}), and pulses (0.03 ± 0.01 Tg CO_2 yr^{-1}) had the highest emissions among the traded crop products.

3.9. Discussion and Conclusions

The total net GHG emissions estimated for South Asia by the bottom-up (BU) and top-down (TD) models for the 2010s were $4,516.4 \pm 639.8$ Tg CO_2 eq yr^{-1} and $4,531.9 \pm 807.5$ $TgCO_2$ eq yr^{-1}. These estimates were 34% and 43% higher than in the 2000s, as well as represent about 8% of the global total GHG emissions, as reported by the IPCC AR6 ($56,600.0 \pm 600.0$ $TgCO_2$ eq yr^{-1}, Dhakal et al., 2022). It is important to note that BU and TD model results for regional total are consistent with each other, as well as they were also consistent with IPCC AR6 estimates of 4,480 $TgCO_2$ eq yr^{-1} (Dhakal et al., 2022). However, spatial patterns can differ (Figure 4). These agreements, among different estimates, suggested a robust understanding of the region's GHG exchanges.

The estimated industrial-related anthropogenic emissions ($E_{Fossil} + E_{CH4\_AP} + E_{N2O\_AP}$) were 3848.1 ± 489.4 Tg CO_2 eq yr^{-1}, which were 85% and 84% of the total fluxes from the BU and TD models, respectively (Figure 1). Approximately 53% (2399.7 ± 427.7 Tg CO_2 eq. yr^{-1}) of the total CO_2 eq. emissions, as calculated by BU models, and 46% (2124.81 ± 641.2 Tg CO_2 eq. yr^{-1}) of the total emissions estimated by TD models were solely of CO_2 emissions. The total CH_4 emission contributions were 31% (1404.27 ± 95.9 Tg CO_2 eq yr^{-1}) and 34% (1531.4 ± 205.2 Tg CO_2 eq. yr^{-1}), and the rest 16% (712.4 ± 466 Tg CO_2 eq yr^{-1}) and 18% (875.7 ± 446 Tg CO_2 eq. yr^{-1}) of the total emissions were N_2O (Figure 3).

Although our study's model results suggest that SA terrestrial ecosystems serve as a net carbon sink for atmospheric CO_2, several recent satellite-based studies report conflicting findings. Some studies suggest that while forests in SA, particularly in countries like India, may function as carbon sources due to climate warming, agricultural ecosystems act as carbon sinks driven by crop expansion and improved management practices.

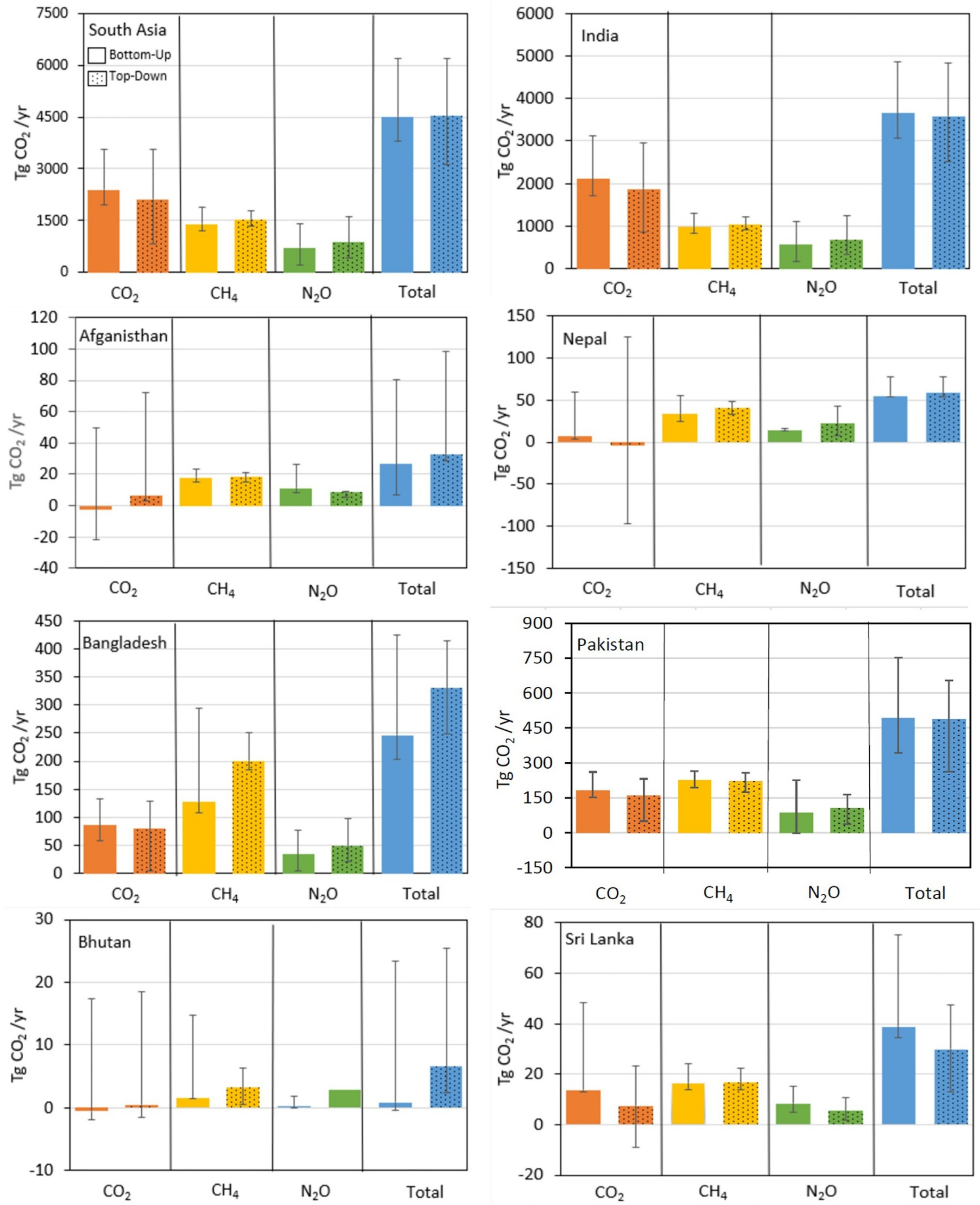

Figure 3. The GHG emission budget for South Asia and its countries is based on the syntheses of the top-down and bottom-up model results and various data sets for the 2010s.

Despite these dynamics, the net primary productivity (NPP) shows limited variation over time (e.g., Das et al., 2020; Park et al., 2023). However, other satellite-based studies show contradictory results regarding NPP. For instance, Bala et al. (2013) attribute rising NPP during the 2000s to CO2 fertilization, while Nayak et al. (2016) and Bejagam and Sharma (2022) link the increase to changes in precipitation. Zeng et al. (2023) further challenge the reliability of satellite data in tropical forest biomes, arguing that complex forest structures cast large shadows, leading to an underestimation of fraction of photosynthetically active radiation (FPAR) and hence GPP and NPP fluxes. Given these substantial uncertainties in model and satellite-based carbon sequestration estimates in South Asia, refining these estimates using enhanced observational data and advanced methods is critical, as detailed below.

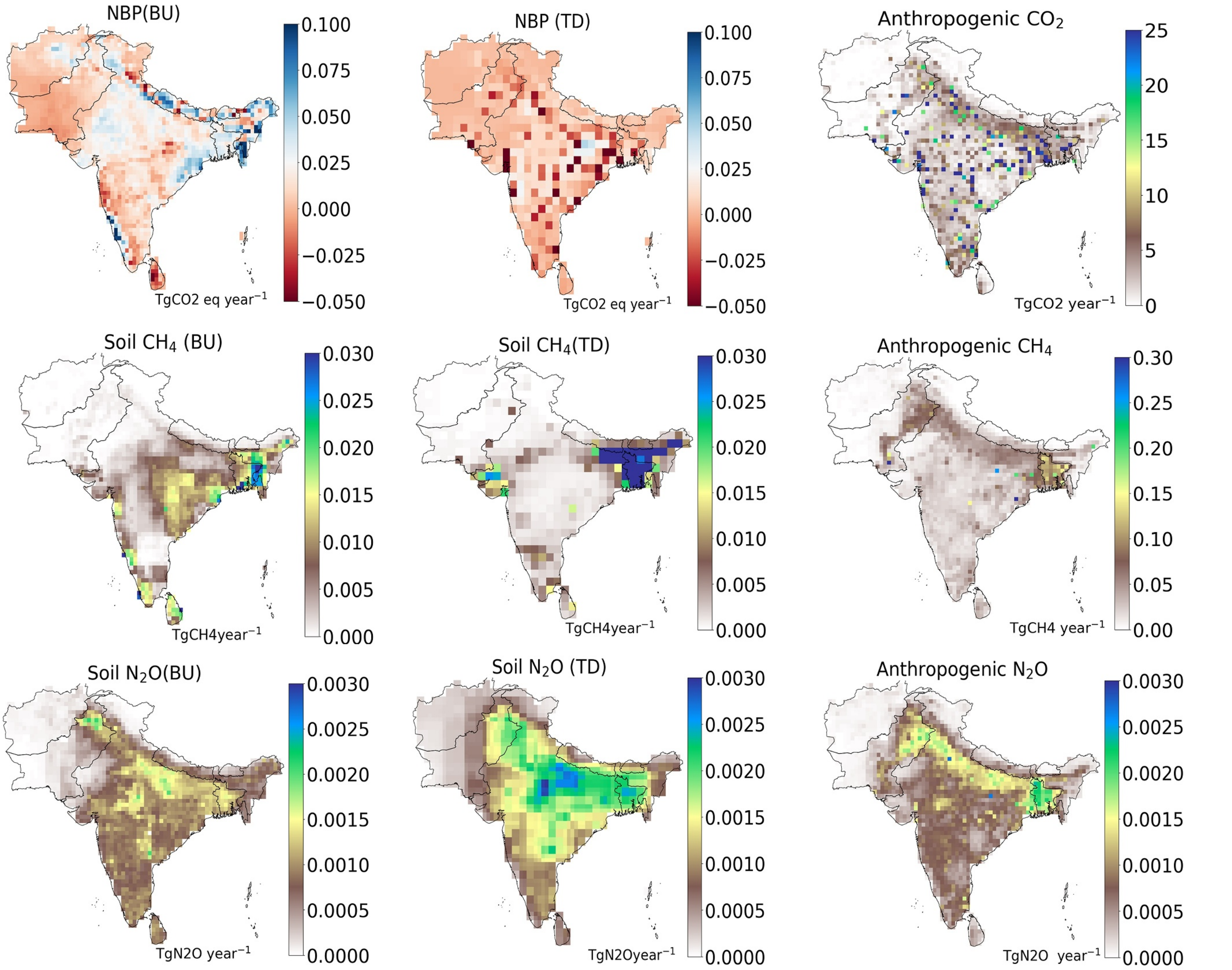

Figure 4. The GHG emissions (CO_2, CH_4, and N_2O) at 0.5 × 0.5 deg grids for South Asia and its countries are based on the syntheses of top-down (TD) and bottom-up (BU) model results and various data sets for the 2010s.

Overall, both TD and BU model results indicate that the regional total E_{NBP} sink fluxes were smaller than the magnitude of the carbon sources, primarily due to the large emissions from the combustion of fossil fuels (Table 1). The SA region's emissions from fossil fuel burning were 11–15 times higher than the region's NBP (Table 1). As a result, the region and its countries, with the exception of Afghanistan and Bhutan, are a net source of CO_2 for TD and BU model-estimated CO_2 fluxes when fossil fuel emissions are accounted for. Afghanistan was a small net sink based on the bottom-up model results, while Bhutan was also a sink for CO_2 based on the top-down model results (Table 1).

In contrast to CO_2 emissions, CH_4 emissions were dominated by enteric fermentation in ruminant livestock and rice cultivation. The major contribution to the total N_2O emissions came from agricultural soils due to fertilizer applications. At a sectoral level, the energy sector contributed 60% of the total GHG emissions, while the agricultural sector contributed around 30%. The rest came from industrial activities, waste management, and land use and land cover activities.

The magnitudes of GHG sources and sink fluxes are different across different countries in the region. For example, India's CO_2 emissions were higher than its CH_4 and N_2O emissions. However, in other countries, CH_4 emissions dominated during the 2010s. This diversity highlights the distinct factors, particularly the socioeconomic factors (e.g., economic growth and population size; Table S8 in Supporting Information S1), of key drivers influencing GHG emissions across South Asian countries because changes in these factors directly influence land cover and land use, industrial and agricultural activities, climatic conditions, frequency of forest fires, and management strategies. For example, with its large population and rapid economic expansion (as indicated by GDP; Table S8 in Supporting Information S1), India is the region's largest emitter of GHG emissions (80%). The primary contributors to India's emissions are industrial activities and energy production, while population growth and increased food demand are further driving LULCC.

Pakistan (11%) and Bangladesh (6%) follow India regarding emissions, with moderate socioeconomic factors at play, albeit at a lower scale. These countries' more moderate economic growth and industrialization rates result in comparatively lower CO_2 emissions than CH_4 emissions (Figure 3). Afghanistan, Nepal, and Sri Lanka exhibit low emissions (1% or less), which are primarily influenced by land use changes, particularly deforestation for agricultural expansion. The slowest pace of economic development in these countries, relative to high emitters like India and Pakistan (Table S8 in Supporting Information S1), contributes to their lower fossil fuel-related emissions (Figure 3). Bhutan stands out for its commitment to maintaining almost a carbon-neutral status, primarily due to its focus on conservation and reliance on renewable energy, particularly hydropower. Bhutan's small population and emphasis on balancing development with sustainability have kept its GHG emissions the lowest in the region (<0.1%) (Figure 3).

This study's country-level GHG emission results can inform decision-makers about GHG emission management and policy development. When assessing emissions for mitigation policies, it is crucial to fully understand these countries' broader environmental and social impacts, including implications for public health, economic challenges, and vulnerabilities to climate change. Higher emissions are associated with deteriorating air quality, which can lead to increased rates of respiratory illnesses, particularly in densely populated countries such as India, Pakistan, and Bangladesh. Deforestation and land use changes in rural areas disrupt local communities' access to natural resources, negatively affecting agriculture and livelihoods. On the economic development front, South Asian countries, all of which are developing, face the challenge of balancing economic growth with environmental sustainability. Adopting cleaner technologies is critical for mitigating the long-term societal impacts of emissions. Furthermore, given the high vulnerability of many South Asian countries to the effects of climate change, such as flooding in Bangladesh, these nations must implement policies that prioritize renewable energy, sustainable land management, and conservation efforts. Bhutan's success in maintaining a carbon-negative status, driven by its focus on renewable energy and environmental conservation, provides a potential model for other countries in the region to explore pathways toward sustainable development while reducing emissions.

At the same time, it is also important to note that the uncertainty associated with regional and country-specific GHG emissions estimates using top-down and bottom-up modeling approaches is substantial, represented here as the one σ standard deviation of the model-derived estimates. The spatial emission patterns for top-down and bottom-up models also differ significantly (Figure 4). Comparing emissions national inventory estimates from the United Nations Framework Convention on Climate Change (UNFCCC, 2024a, 2024b) with emissions based on top-down and bottom-up models in the present study reveals diverse patterns across different countries in SA (Table 7). UNFCCC's national emission inventories generally align within the large ranges provided by either or both BU and TD models. Some countries like Pakistan and Sri Lanka exhibit instances where UNFCCC's inventory values align more closely with BU estimates. However, the emission inventories for a country like India deviate the most from the broader ranges provided by both models' estimates. This discrepancy between UNFCCC-reported values and top-down and bottom-up model estimated values highlights the complexity and challenges associated with model estimating and reporting GHG emissions and the importance of improving data quality, methodological consistency, and transparency in emission accounting practices.

According to our analysis, GHG emissions from terrestrial ecosystems are less reliable than those from anthropogenic non-terrestrial sources. In particular, the terrestrial net CO_2 flux terms, E_{NBP_BU} and E_{NBP_TD}, show the highest uncertainty, with estimates of -170.2 ± 279.0 and -210.4 ± 504.9 Tg CO_2 yr^{-1}, respectively. This high uncertainty primarily arises from emissions related to deforestation and other disturbances. Additional uncertainty stems from post-disturbance recovery sinks and interannual variations caused by climate anomalies across South Asian countries. In contrast, CO_2 E_{Fossil} emissions are the most certain, with an estimated value of 2335.4 ± 117.0 Tg CO_2 yr^{-1}. This is because fossil fuel consumption (coal, oil, and natural gas) is well-

Table 7
Comparison of UNFCCC-Reported Country-Specific Total Emission Inventories ($TgCO_2\ eq\ yr^{-1}$) (UNFCCC, 2024a, 2024b) Mean for the Random Periods With the Top-Down (TD) and Bottom-Up (BU) Models and Their Uncertainty Ranges

	UNFCCC			This study	
Country	Method[a]	Period/Year	Emissions	BU	TD
Afghanistan	NC	2012–2013	60.2	44.9 (15.6–74.4)	42.3 (30.7–53.9)
	BUR	2010–2017	40.4	57.5(33.6–81.5)	46.8(18.5–75.2)
Bangladesh	NC	2010–2012	152.3	208.5 (169.3–247.8)	199.2 (146.6–251.8)
	BUR	2013–2019	193.8	236.0 (193.6–279.6)	315.5 (248.4–382.6)
Bhutan	NC	2010–2015	−5.7	2.8 ((−3)–8.5)	6.12 ((−5.1)–17.3)
	BUR	2010–2019	−6.5	0.9 ((−2.9)–4.7)	6.5 ((−2.6)–15.7)
India	NC	2011–2019	2394.7	3343 (3048.5–3637.5)	3568.8 (3054.4–4,083.4)
	BUR	2011–2016	2271.6	3236.9 (2754.2–3719.5)	3437.6 (2913.5–3961.9)
Nepal	NC	2010–2011	28.2	41 (12.4–69.6)	49.4 (27.1–71.7)
	BUR	–	–	–	–
Pakistan	NC	2012–2015	405.0	426.8 (365.7–487.8)	454 (406.7–501.5)
	BUR	2012,2015,2018	359.6	481.8 (381.7–581.9)	503.3(397.3–609.3)
Sri Lanka	NC	2010	3.7	10.1 ((−6.6)–26.9)	27.2 (16.1–38.2)
	BUR	–	–	–	–

[a]"NC" values are based on National Communication (NC) submissions from Non-Annex I Parties (UNFCCC, 2024a), and Biennial Update Report (BUR) values are based on BUR submissions from Non-Annex I Parties (UNFCCC, 2024b).

documented through detailed records of energy production, trade, and usage, as well as countries and industries regularly update their emissions data (Crippa, Guizzardi et al., 2020; Crippa, Solazzo et al., 2020).

The existing TD and BU methods for modeling GHG emissions require effective enhancements to incorporate sub-grid scale processes and feedback loops. The coarse spatial resolution of TD and (to a lesser extent) BU models introduce significant uncertainties in their results. Low-resolution models often fail to capture critical fine-scale processes, such as local climate variations, topography, vegetation types, and land-use patterns. This oversimplification can obscure complex interactions between land and climate systems, reducing the models' ability to accurately simulate regional and localized phenomena, such as extreme weather events, microclimates, and ecosystem responses. Moreover, BU models must account for key agricultural management practices, including irrigation and nitrogen fertilizer application. Without incorporating these factors, models underestimate carbon sequestration rates in agricultural landscapes. Another critical regional gap is the lack of Fluxnet tower data for biophysical and micrometeorological variables. These data are essential for validating model and satellite-derived results, but they remain entirely absent in many South Asian areas.

Future GHG emission analyses will require comprehensive data sets on environmental variables, notably LULCC activities at finer resolutions. This entails considering intricate decisions regarding land management at a sub-national level, given the diverse land classes, soil types, commodities, and myriad management options prevalent in most countries.

To improve the accuracy of satellite-derived estimates of terrestrial carbon fluxes, studies must consider using finer-resolution satellite data, such as Landsat, which offers 30-m resolution (Mondal et al., 2020). Currently, many studies rely on coarser resolution data from satellites like MODIS, which struggle to detect long-term changes, such as greening trends and carbon sequestration dynamics, and often fail to capture the slow degradation of tropical forests. This challenge is particularly pronounced in tropical regions, where deep convective clouds frequently interfere with data retrieval, leading to poor performance of satellite-based estimates (Deb Burman et al., 2020).

Using satellite-derived biomass and other GHG products can also provide opportunities to reduce uncertainties. Utilizing higher-resolution data alongside advanced process-based modeling, both TD and BU, will be pivotal in accurately capturing carbon and other GHG dynamics. Top-down models estimating the budget for the SA are notably under-constrained by data, primarily due to the significant lack of greenhouse gas (GHG) and climate measurement data in this area (Chandra et al., 2021; Patra et al., 2016). Such approaches will enable a deeper understanding of GHG stocks and flows, establish crucial connections to ground-based physical processes and the national GHG inventories, and facilitate more informed policy decisions.

Conflict of Interest

The authors declare no conflicts of interest relevant to this study.

Data Availability Statement

All model output datasets analyzed in this study are publicly available. Tables S1–S7 in Supporting Information S1 provide citations for the original data sources, with full citations listed in the References section.

Acknowledgments

We gratefully thank the following data providers and model developers for their continuous efforts and for sharing their data: the Global Carbon Project (GCP); Regional Carbon Cycle Assessment Pricesses 2 (RECCAP-2); and the TRENDY experiment version 11, which included the models CABLE POP, CLASSIC, CLM5, DLEM, IBIS, ISAM, JSBACH, JULES, LPJ, LJP-GUESS, LPX-Bern, OCN, ORCHIDEE, SDGVM, VISIT, and YJB. We thank Z. Deng of Tsinghua University and L. Hu of Zhejiang University for their assistance in compiling the UNFCCC emission inventory data. We also thank Pengyue Du for data compilation and figure preparation. AK Jain and S Seshadri are partly supported by the NASA LCLUC Program (award 80NSSC24K0920). AK Jain also acknowledged a NASA project (80NSSC22K1363) for supporting travel to a meeting in India on LCLUC in South Asian. NC and PKP are supported by the Arctic Challenge for Sustainability II (ArCS-II) project (Grant JPMXD1420318865) and the Environmental and Technology Development Fund (JPMEERF21S20800) of the Environmental Restoration and Conservation Agency of Japan.

References

Bala, G., Joshi, J., Chaturvedi, R. K., Gangamani, H. V., Hashimoto, H., & Nemani, R. (2013). Trends and variability of AVHRR-derived NPP in India. *Remote Sensing*, *5*(2), 810–829. https://doi.org/10.3390/rs5020810

Bejagam, V., & Sharma, A. (2022). Impact of climatic changes and anthropogenic activities on ecosystem net primary productivity in India during 2001–2019. *Ecological Informatics*, *70*, 101732. https://doi.org/10.1016/j.ecoinf.2022.101732

Canadell, J. G., Monteiro, P. M., Costa, M. H., Da Cunha, L. C., Cox, P. M., Alexey, V., et al. (2021). *Global carbon and other biogeochemical cycles and feedbacks. IPCC AR6 WGI, Final Government Distribution*. Cambridge University Press. https://doi.org/10.1017/9781009157896.007

Cervarich, M., Shu, S., Jain, A. K., Arneth, A., Canadell, J., Friedlingstein, P., et al. (2016). The terrestrial carbon budget of South and Southeast Asia. *Environmental Research Letters*, *11*(10), 105006. https://doi.org/10.1088/1748-9326/11/10/105006

Chandra, N., Patra, P. K., Bisht, J. S. H., Ito, A., Umezawa, T., Saigusa, N., et al. (2021). Emissions from the oil and gas sectors, coal mining and ruminant farming drive methane growth over the past three decades. *Journal of the Meteorological Society of Japan. Ser. II*, *99*(2), 2021–3015. https://doi.org/10.2151/jmsj.2021-015

Chaturvedi, R. K., Roy, A., Karmakar, S., & Ghosh, S. (2023). Warming inhibits increases in vegetation net primary productivity despite greening in India. *Scientific Reports*, *13*(1), 21309. https://doi.org/10.1038/s41598-023-48614-3

Ciais, P., Bastos, A., Chevallier, F., Lauerwald, R., Poulter, B., Canadell, J. G., et al. (2022). Definitions and methods to estimate regional land carbon fluxes for the second phase of the REgional Carbon Cycle Assessment and Processes Project (RECCAP-2). *Geoscientific Model Development*, *15*(3), 1289–1316. https://doi.org/10.5194/gmd-15-1289-2022

Crippa, M., Guizzardi, D., Muntean, M., Schaaf, E., Solazzo, E., Monforti-Ferrario, F., et al. (2020). *Fossil CO_2 emissions of all world countries - 2020 Report, EUR 30358 EN*. Publications Office of the European Union. https://doi.org/10.2760/56420

Crippa, M., Guizzardi, D., Solazzo, E., Muntean, M., Schaaf, E., Monforti-Ferrario, F., et al. (2021). *GHG emissions of all world countries*. Publications Office of the European Union. Retrieved from https://www.researchgate.net/profile/Fabio-Monforti/publication/355369128_GHG_emissions_of_all_world_countries_booklet_2021report/links/616d32a3951b3574c65e2d4b/GHG-emissions-of-all-world-countries-booklet-2021report.pdf

Crippa, M., Solazzo, E., Huang, G., Guizzardi, D., Koffi, E., Muntean, M., et al. (2020). High resolution temporal profiles in the emissions Database for global atmospheric research. *Scientific Data*, *7*, 1–17. https://doi.org/10.1038/s41597-020-0462-2Das

Deb Burman, P. K., Sarma, D., Chakraborty, S., Karipot, A., & Jain, A. K. (2020). The effect of Indian summer monsoon on the seasonal variation of carbon sequestration by a forest ecosystem over North-East India. *SN Applied Sciences*, *2*, 154. https://doi.org/10.1007/s42452-019-1934-x

Deng, Z., Ciais, P., Tzompa-Sosa, Z. A., Saunois, M., Qiu, C., Tan, C., et al. (2022). Comparing national greenhouse gas budgets reported in UNFCCC inventories against atmospheric inversions. *Earth System Science Data*, *14*(4), 1639–1675. https://doi.org/10.5194/essd-14-1639-2022

Dhakal, S., Minx, J. C., Toth, F. L., Abdel-Aziz, A., Figueroa Meza, M. J., Hubacek, K., et al. (2022). Emissions trends and drivers. In *IPCC, 2022: Climate change 2022: Mitigation of climate change. Contribution of working group III to the IPCC AR6 WGIII*. Cambridge University Press. https://doi.org/10.1017/9781009157926.004

Dlugokencky, E., & Tans, P. (2022). *Trends in atmospheric carbon dioxide*. National Oceanic and Atmospheric Administration, Global Monitoring Laboratory (NOAA/GML). Retrieved from https://gml.noaa.gov/ccgg/trends/

Dlugokencky, E. J., Nisbet, E. G., Fisher, R., & Lowry, D. (2011). Global atmospheric methane: Budget, changes and dangers. *Philosophical transactions of the royal society A: Mathematical, physical and engineering sciences* (Vol. 369(1943), 2058–2072). https://doi.org/10.1098/rsta.2010.0341

Etheridge, D. M., Pearman, G. I., & Fraser, P. J. (1992). Changes in tropospheric methane between 1841 and 1978 from a high accumulation-rate Antarctic ice core. *Tellus B: Chemical and Physical Meteorology*, *44*(4), 282–294. https://doi.org/10.1034/j.1600-0889.1992.t01-3-00006.x

FAOSTAT. (2024). Data for Wood and Crop trade was downloaded on 03/5/2024. Retrieved from https://www.fao.org/faostat/en/#data

Friedlingstein, P., Jones, M. W., Sullivan, M. O., Andrew, R. M., Bakker, D. C. E., Hauck, J., et al. (2022). Global carbon budget 2021. *14*, 1917–2005. https://doi.org/10.5194/essd-14-1917-2022

Gasser, T., Crepin, L., Quilcaille, Y., Houghton, R. A., Ciais, P., & Obersteiner, M. (2020). Historical CO_2 emissions from land use and land cover change and their uncertainty. *Biogeosciences*, *17*(15), 4075–4101. https://doi.org/10.5194/bg-17-4075-2020

Ghosh, A., Patra, P. K., Ishijima, K., Umezawa, T., Ito, A., Etheridge, D. M., et al. (2015). Variations in global methane sources and sinks during 1910-2010. *Atmospheric Chemistry and Physics*, *15*(5), 2595–2612. https://doi.org/10.5194/acp-15-2595-2015

Goldewijk, K. K., Beusen, A., Doelman, J., & Stehfest, E. (2017). Anthropogenic land use estimates for the Holocene - HYDE 3.2. *Earth System Science Data*, *9*(2), 927–953. https://doi.org/10.5194/essd-9-927-2017

Gumma, M. K., Nelson, A., Thenkabail, P., & Singh, A. (2011). Mapping rice areas of South Asia using MODIS multitemporal data. *Journal of Applied Remote Sensing*, *5*(1), 053547. https://doi.org/10.1117/1.3619838

Hansis, E., Davis, S. J., & Pongratz, J. (2015). Relevance of methodological choices for accounting of land use change carbon fluxes. *Global Biogeochemical Cycles*, *29*, 1230–1246. https://doi.org/10.1002/2014GB004997

Hoor, P., Borken-Kleefeld, J., Caro, D., Dessens, O., Endresen, O., Gauss, M., et al. (2009). The impact of traffic emissions on atmospheric ozone and OH: Results from QUANTIFY. *Atmospheric Chemistry and Physics*, *9*, 3113–3136. https://doi.org/10.5194/acp-9-3113-2009

Houghton, R. A., & Nassikas, A. A. (2017). Global and regional fluxes of carbon from land use and land cover change 1850-2015: Carbon emissions from land use. *Global Biogeochemical Cycles*, *31*(3), 456–472. https://doi.org/10.1002/2016GB005546

Houweling, S., Bergamaschi, P., Chevallier, F., Heimann, M., Kaminski, T., Krol, M., et al. (2017). Global inverse modeling of CH_4 sources and sinks: An overview of methods. *Atmospheric Chemistry and Physics*, *17*(1), 235–256. https://doi.org/10.5194/acp-17-235-2017

IPCC. (2014). Synthesis report. Contribution of working groups I, II and III to the fifth assessment report of the intergovernmental panel on climate change. *IPCC*, 151.

IPCC. (2021). In *Climate change 2021: The physical science basis. Contribution of working group I to the sixth assessment report of the intergovernmental panel on climate change* (Eds.), V. Masson-Delmotte, P. Zhai, A. Pirani, S. L. Connors, C. Péan, et al., Cambridge University Press. https://doi.org/10.1017/9781009157896

Lauerwald, R., Allen, G. H., Deemer, B. R., Liu, S., Maavara, T., Raymond, P., et al. (2023a). Inland water greenhouse gas budgets for RECCAP2: 1. State-of-the-art of global scale assessments. *Global Biogeochemical Cycles*, *37*(5), e2022GB007657. https://doi.org/10.1029/2022GB007657

Lauerwald, R., Allen, G. H., Deemer, B. R., Liu, S., Maavara, T., Raymond, P., et al. (2023b). Inland water greenhouse gas budgets for RECCAP2: 2. Regionalization and homogenization of estimates. *Global Biogeochemical Cycles*, *37*(5), e2022GB007658. https://doi.org/10.1029/2022GB007658

Meehl, G. A., Covey, C., Delworth, T., Latif, M., McAvaney, B., Mitchell, J. F., et al. (2007). The WCRP CMIP3 multimodel dataset: A new era in climate change research. *Bulletin of the American Meteorological Society*, *88*(9), 1383–1394. https://doi.org/10.1175/bams-88-9-1383

Melton, J. R., Wania, R., Hodson, E. L., Poulter, B., Ringeval, B., Spahni, R., et al. (2013). Present state of global wetland extent and wetland methane modelling: Conclusions from a model inter-comparison project (WETCHIMP). *Biogeosciences*, *10*(2), 753–788. https://doi.org/10.5194/bg-10-753-2013

Minx, J. C., Lamb, W. F., Andrew, R. M., Canadell, J. G., Crippa, M., Döbbeling, N., et al. (2021). A comprehensive and synthetic dataset for global, regional, and national greenhouse gas emissions by sector 1970 – 2018 with an extension to 2019. *Earth System Science Data*, *13*(11), 5213–5252. https://doi.org/10.5194/essd-13-5213-2021

Mondal, P., McDermid, S. S., & Qadir, A. (2020). A reporting framework for sustainable development goal 15: Multi-scale monitoring of forest degradation using MODIS, Landsat and Sentinel data. *Remote Sensing of Environment*, *237*, 111592. https://doi.org/10.1016/j.rse.2019.111592

Nayak, R. K., Mishra, N., Dadhwal, V. K., Patel, N. R., Salim, M., Rao, K. H., & S Dutt, C. B. (2016). Assessing the consistency between AVHRR and MODIS NDVI datasets for estimating terrestrial net primary productivity over India. *Journal of Earth System Science*, *125*(6), 1189–1204. https://doi.org/10.1007/s12040-016-0723-9

Park, T., Gumma, M. K., Wang, W., Panjala, P., Dubey, S. K., & Nemani, R. R. (2023). Greening of human-dominated ecosystems in India. *Communications Earth & Environment*, *4*(1), 419. https://doi.org/10.1038/s43247-023-01078-9

Patra, P. K., Canadell, J. G., Houghton, R. A., Piao, S. L., Oh, N., Ciais, P., et al. (2013). The carbon budget of South Asia. *Biogeosciences*, *10*(1), 513–527. https://doi.org/10.5194/bg-10-513-2013

Patra, P. K., Saeki, T., Dlugokencky, E. J., Ishijima, K., Umezawa, T., Ito, A., et al. (2016). Regional methane emission estimation based on observed atmospheric concentrations (2002–2012). *Journal of the Meteorological Society of Japan*, *94*(1), 85–107. https://doi.org/10.2151/jmsj.2016-006

Peters, G. P., Davis, S. J., & Andrew, R. (2012). A synthesis of carbon in international trade. *Biogeosciences*, *9*(8), 3247–3276. https://doi.org/10.5194/bg-9-3247-2012

Pingali, P. L. (2012). Green Revolution: Impacts, limits, and the path ahead. *Proceedings of National Academic of Sciences* (Vol. 109(31), 12302–12308). https://doi.org/10.1073/pnas.0912953109

Poulter, B., Bousquet, P., Canadell, J. G., Ciais, P., Peregon, A., Saunois, M., et al. (2017). Global wetland contribution to 2000-2012 atmospheric methane growth rate dynamics. *Environmental Research Letters*, *12*(9), 094013. https://doi.org/10.1088/1748-9326/aa8391

Raghuram, N., Sutton, M. A., Jeffery, R., Ramachandran, R., & Adhya, T. K. (2021). From South Asia to the world: Embracing the challenge of global sustainable nitrogen management. *One Earth*, *4*(1), 22–27. https://doi.org/10.1016/j.oneear.2020.12.017

Saunois, M., Stavert, A. R., Poulter, B., Bousquet, P., Canadell, J. G., Jackson, R. B., et al. (2020). The global methane budget 2000 – 2017. *Earth System Science Data*, *12*(3), 1561–1623. https://doi.org/10.5194/essd-12-1561-2020

Sitch, S., Friedlingstein, P., Gruber, N., Jones, S. D., Murray-Tortarolo, G., Ahlström, A., et al. (2015). Recent trends and drivers of regional sources and sinks of carbon dioxide. *Biogeosciences*, *12*(3), 653–679. https://doi.org/10.5194/bg-12-653-2015

Tian, H., Pan, N., Thompson, R. L., Canadell, J. G., Suntharalingam, P., Regnier, P., et al. (2024). Global nitrous oxide budget 1980–2020. *Earth System Science Data*, *16*(6), 2543–2604. https://doi.org/10.5194/essd-16-2543-2024

Tian, H., Xu, R., Canadell, J. G., Thompson, R. L., Winiwarter, W., Suntharalingam, P., et al. (2020). A comprehensive quantification of global nitrous oxide sources and sinks. *Nature*, *586*(7828), 248–256. https://doi.org/10.1038/s41586-020-2780-0

United Nations Framework Convention on Climate Change (UNFCCC). (2015). Paris agreement to the United Nations framework convention on climate change, Dec. 12, 2015, T.I.A.S. No. 16-1104. Retrieved from https://unfccc.int/sites/default/files/english_paris_agreement.pdf

United Nations Framework Convention on Climate Change (UNFCCC). (2021). In *Official document of the 26th Conference of the Parties (COP26) to the United Nations Framework Convention on Climate Change (UNFCCC), UNFCCC/CP/2021/1/Add.1*. Retrieved from https://unfccc.int/documents/306810

United Nations Framework Convention on Climate Change (UNFCCC). (2024b). Biennial update report submissions from non-Annex I Parties. Retrieved from https://unfccc.int/BURs

United Nations Framework Convention on Climate Change (UNFCCC). (2024a). National communication submissions from non-annex I Parties. Retrieved from https://unfccc.int/non-annex-I-NCs

van der Werf, G. R., Randerson, J. T., Giglio, L., van Leeuwen, T. T., Chen, Y., Rogers, B. M., et al. (2017). Global fire emissions estimates during 1997-2016. *Earth System Science Data*, *9*(2), 697–720. https://doi.org/10.5194/essd-9-697-2017

Viovy, N. (2018). CRUNCEP version 7-atmospheric forcing data for the community land model. *Research Data Archive National Center for Atmospheric Research Computational Information Systems Lab*, *10*. https://doi.org/10.5065/PZ8F-F017

Weigel, A. P., Liniger, M. A., & Appenzeller, C. (2008). Can multi-model combination really enhance the prediction skill of probabilistic ensemble forecasts? *Quarterly Journal of the Royal Meteorological Society*, *134*(630), 241–260. https://doi.org/10.1002/qj.210

World Bank Group. (2023). *World development indicators 2023*. World Bank Publications. Retrieved from https://data.worldbank.org/?locations=8S-AF

Xu, X., Sharma, P., Shu, S., Lin, T.-Z., Ciais, P., Tubiello, F., et al. (2021). Global greenhouse gas emissions from plant- and animal-based food. *Nature Food*, *2*, 723–732. https://doi.org/10.1038/s43016-021-00358-x

Zeng, Y., Hao, D., Park, T., Zhu, P., Huete, A., Myneni, R., et al. (2023). Structural complexity biases vegetation greenness measures. *Nature Ecology & Evolution*, *7*(11), 1–9. https://doi.org/10.1038/s41559-023-02187-6

References From the Supporting Information

Arora, V. K., Melton, J. R., & Plummer, D. (2018). An assessment of natural methane fluxes simulated by the CLASS-CTEM model (pp. 4683–4709).

Bergamaschi, P., Houweling, S., Segers, A., Krol, M., Frankenberg, C., Scheepmaker, R. A., et al. (2013). Atmospheric CH_4 in the first decade of the 21st century: Inverse modeling analysis using SCIAMACHY satellite retrievals and NOAA surface measurements. *Journal of Geophysical Research: Atmospheres*, *118*(13), 7350–7369. https://doi.org/10.1002/jgrd.50480

Bergamaschi, P., Karstens, U., Manning, A. J., Saunois, M., Tsuruta, A., & Berchet, A. (2018). Inverse modelling of European CH 4 emissions during 2006 – 2012 using different inverse models and reassessed atmospheric observations (pp. 901–920).

Bergamaschi, P., Krol, M., Meirink, J. F., Dentener, F., Segers, A., Aardenne, J. V., et al. (2012). Inverse modeling of European CH_4 emissions 2001 – 2006 115. *Journal of Geophysical Research*, *115*(D22), 1–18. https://doi.org/10.1029/2010JD014180

Haverd, V., Smith, B., Nieradzik, L., Briggs, P. R., Woodgate, W., Trudinger, C. M., et al. (2018). A new version of the CABLE land surface model (Subversion revision r4601) incorporating land use and land cover change, woody vegetation demography, and a novel optimisation-based approach to plant coordination of photosynthesis. *Geoscientific Model Development*, *11*(7), 2995–3026. https://doi.org/10.5194/gmd-11-2995-2018

Hayman, G. D., Connor, F. M. O., Dalvi, M., Clark, D. B., Gedney, N., Huntingford, C., et al. (2014). Comparison of the HadGEM2 climate-chemistry model against in situ and SCIAMACHY atmospheric methane data. 13257–13280. https://doi.org/10.5194/acp-14-13257-2014

Ishizawa, M., Mabuchi, K., Shirai, T., Inoue, M., Morino, I., Uchino, O., et al. (2016). Inter-annual variability of summertime CO2 exchange in Northern Eurasia inferred from GOSAT XCO2. *Environmental Research Letters*, *11*(10), 105001. https://doi.org/10.1088/1748-9326/11/10/105001

Ito, A., & Inatomi, M. (2012). Use of a process-based model for assessing the methane budgets of global terrestrial ecosystems and evaluation of uncertainty. *Biogeosciences*, *9*(2), 759–773. https://doi.org/10.5194/bg-9-759-2012

Jain, A. K., Meiyappan, P., Song, Y., & House, J. I. (2013). CO2 emissions from land-use change affected more by nitrogen cycle, than by the choice of land-cover data. *Global Change Biology*, *19*(9), 2893–2906. https://doi.org/10.1111/gcb.12207

Kato, E., Kinoshita, T., Ito, A., Kawamiya, M., & Yamagata, Y. (2013). Evaluation of spatially explicit emission scenario of land-use change and biomass burning using a process-based biogeochemical model. *Journal of Land Use Science*, *8*(1), 104–122. https://doi.org/10.1080/1747423X.2011.628705

Kleinen, T., Mikolajewicz, U., & Brovkin, V. (2020). Terrestrial methane emissions from the Last Glacial Maximum to the preindustrial period. *Climate of the Past*, *1*(2), 575–595. https://doi.org/10.5194/cp-16-575-2020

Lawrence, D. M., Fisher, R. A., Koven, C. D., Oleson, K. W., Swenson, S. C., Bonan, G., et al. (2019). The Community Land Model version 5: Description of new features, benchmarking, and impact of forcing uncertainty. *Journal of Advances in Modeling Earth Systems*, *11*(12), 4245–4287. https://doi.org/10.1029/2018ms001583

Liu, J., You, Y., Li, J., Sitch, S., Gu, X., Nabel, J. E. M. S., et al. (2021). Response of global land evapotranspiration to climate change, elevated CO_2, and land use change. *Agricultural and Forest Meteorology*, *311*, 108663. https://doi.org/10.1016/j.agrformet.2021.108663

Maksyutov, S., Mabuchi, K., Shirai, T., Inoue, M., Morino, I., Uchino, O., et al. (2016). Inter-annual variability of summertime CO2 exchange in Northern Eurasia inferred from GOSAT XCO2. *Environmental Research Letters*, *11*(10), 105001. https://doi.org/10.1088/1748-9326/11/10/105001

Mcguire, A. D., Christensen, T. R., Hayes, D., Heroult, A., Euskirchen, E., Kimball, J. S., et al. (2012). An assessment of the carbon balance of arctic tundra: Comparisons among observations, process models. Atmospheric Inversions. *Biogeosciences*, *1*, 3185–3204. https://doi.org/10.5194/bg-9-3185-2012

Melton, J. R., Arora, V. K., Wisernig-Cojoc, E., Seiler, C., Fortier, M., Chan, E., & Teckentrup, L. (2020). Model v1.0: The open-source community successor to the Canadian Land Surface Scheme (CLASS) and the Canadian Terrestrial Ecosystem Model (CTEM)-Part 1: Model framework and site-level performance. *Geoscientific Model Development*, *13*, 2825–2850. https://doi.org/10.5194/gmd-13-2825-2020

Niwa, Y., Fujii, Y., Sawa, Y., Iida, Y., Ito, A., Satoh, M., et al. (2017a). A 4D-Var inversion system based on the icosahedral grid model (NICAM-TM 4D-Var v1.0) - Part 2: Optimization scheme and identical twin experiment of atmospheric CO2 inversion. *Geoscientific Model Development*, *10*(6), 2201–2219. https://doi.org/10.5194/gmd-10-2201-2017

Niwa, Y., Tomita, H., Satoh, M., Imasu, R., Sawa, Y., Tsuboi, K., et al. (2017b). A 4D-Var inversion system based on the icosahedral grid model (NICAM-TM 4D-Var v1.0)-Part 1: Offline forward and adjoint transport models. *Geoscientific Model Development*, *10*(3), 1157–1174. https://doi.org/10.5194/gmd-10-1157-2017

Patra, P. K., Dlugokencky, E. J., Elkins, J. W., Dutton, G. S., Tohjima, Y., Sasakawa, M., et al. (2022). Forward and inverse modelling of atmospheric nitrous oxide using MIROC4-atmospheric chemistry-transport model. *Journal of the Meteorological Society of Japan*, *100*(2), 361–386. https://doi.org/10.2151/jmsj.2022-018

Patra, P. K., & Kort, E. A. (2016). Regional methane emission estimation based on observed atmospheric concentrations. *Journal of the Meteorological Society of Japan. Ser. II*, 2002–2012. https://doi.org/10.2151/jmsj.2016-006

Patra, P. K., Takigawa, M., Watanabe, S., Chandra, N., Ishijima, K., & Yamashita, Y. (2018). Improved chemical tracer simulation by MIROC4.0-based atmospheric chemistry-transport model (MIROC4-ACTM). *Scientific Online Letters on the Atmosphere.*, *14*(0), 91–96. https://doi.org/10.2151/SOLA.2018-016

Ringeval, B., Friedlingstein, P., Koven, C., Ciais, P., de Noblet-Ducoudré, N., Decharme, B., & Cadule, P. (2011). Climate-CH4 feedback from wetlands and its interaction with the climate-CO2 feedback 2137–2157. *Biogeosciences*, *8*(8), 2137–2157. https://doi.org/10.5194/bg-8-2137-2011

Spahni, R., Wania, R., Neef, L., Van Weele, M., Pison, I., Bousquet, P., et al. (2011). Constraining global methane emissions and uptake by ecosystems. *Biogeosciences*, *8*(6), 1643–1665. https://doi.org/10.5194/bg-8-1643-2011

Thompson, R. L., Chevallier, F., Crotwell, A. M., Dutton, G., Langenfelds, R. L., Prinn, R. G., et al. (2014). Nitrous oxide emissions 1999 to 2009 from a global atmospheric inversion. *Atmospheric Chemistry and Physics*, *14*(4), 1801–1817. https://doi.org/10.5194/acp-14-1801-2014

Tian, H., Lu, C., Yang, J., Banger, K., Huntzinger, D. N., Schwalm, C. R., et al. (2015a). Global patterns and controls of soil organic carbon dynamics as simulated by multiple terrestrial biosphere models: Current status and future directions. *Global Biogeochemical Cycles*, *29*(6), 775–792. https://doi.org/10.1002/2014gb005021

Tian, H., Ren, W., Yang, J., Tao, B., Cai, W., Lohrenz, S. E., et al. (2015b). Climate extremes dominating seasonal and interannual variations in carbon export from the Mississippi River Basin. *Global Biogeochemical Cycles*, *29*(9), 1333–1347. https://doi.org/10.1002/2014gb005068

Tsuruta, A., Aalto, T., Backman, L., Hakkarainen, J., Van Der Laan-Luijkx, I. T., Krol, M. C., et al. (2017). The CarbonTracker data Assimilation Shell (CTDAS) v1.0: Implementation and global carbon balance 2001-2015. *Geoscientific Model Development*, *10*(7), 2785–2800. https://doi.org/10.5194/gmd-10-2785-2017

Walker, A. P., Quaife, T., van Bodegom, P. M., De Kauwe, M. G., Keenan, T. F., Joiner, J., et al. (2017). The impact of alternative trait-scaling hypotheses for the maximum photosynthetic carboxylation rate (Vcmax) on global gross primary production. *New Phytologist*, *215*(4), 1370–1386. https://doi.org/10.1111/nph.14623

Wells, K. C., Millet, D. B., Bousserez, N., Henze, D. K., Chaliyakunnel, S., Griffis, T. J., et al. (2015). Simulation of atmospheric N 2 O with GEOS-Chem and its adjoint: Evaluation of observational constraints. *Geoscientific Model Development*, *8*(10), 3179–3198. https://doi.org/10.5194/gmd-8-3179-2015

Wilson, C., Chipperfield, M. P., Gloor, M., & Chevallier, F. (2014). Development of a variational flux inversion system (INVICAT v1. 0) using the TOMCAT chemical transport model. *Geoscientific Model Development*, *7*(5), 2485–2500. https://doi.org/10.5194/gmd-7-2485-2014

Yin, Y., Chevallier, F., Ciais, P., Broquet, G., Pison, I., Saunois, M., et al. (2015). Decadal trends in global CO emissions as seen by MOPITT 13433–13451. *Atmospheric Chemistry and Physics*, *15*(23), 13433–13451. https://doi.org/10.5194/acp-15-13433-2015

Yuan, W., Liu, D., Dong, W., Liu, S., Zhou, G., Yu, G., et al. (2014). Multiyear precipitation reduction strongly decreases carbon uptake over northern China. *Journal of Geophysical Research: Biogeosciences*, *119*(5), 881–896. https://doi.org/10.1002/2014JG002608

Yue, X., & Unger, N. (2015). The Yale Interactive terrestrial Biosphere model version 1.0: Description, evaluation and implementation into NASA GISS ModelE2. *Geoscientific Model Development*, *8*, 2399–2417. https://doi.org/10.5194/gmd-8-2399-2015

Zaehle, S., & Friend, A. D. (2010). Carbon and nitrogen cycle dynamics in the O-CN land surface model: 1. Model description, site-scale evaluation, and sensitivity to parameter estimates. *Global Biogeochemical Cycles*, *24*, 1–13. https://doi.org/10.1029/2009GB003521

Zhu, Q., Riley, W. J., Tang, J., Collier, N., Hoffman, F. M., Yang, X., & Bisht, G. (2019). Representing nitrogen, Phosphorus, and carbon interactions in the E3SM land model: Development and global benchmarking. *Journal of Advances in Modeling Earth Systems*, *11*(7), 2238–2258. https://doi.org/10.1029/2018MS001571